

High-Frequency Instabilities of Stokes Waves

Ryan P. Creedon¹, Bernard Deconinck², Olga Trichtchenko³

July 23, 2021

¹Department of Applied Mathematics, University of Washington, Seattle, WA, USA, creedon@uw.edu

²Department of Applied Mathematics, University of Washington, Seattle, WA, USA, deconinc@uw.edu

³Department of Physics and Astronomy, The University of Western Ontario, London, ON, CA, otrichtc@uwo.ca

This paper is dedicated to Harvey Segur, on the occasion of his 80th birthday.

Abstract

Euler's equations govern the behavior of gravity waves on the surface of an incompressible, inviscid, and irrotational fluid of arbitrary depth. We investigate the spectral stability of sufficiently small-amplitude, one-dimensional Stokes waves, *i.e.*, periodic gravity waves of permanent form and constant velocity, in both finite and infinite depth. We develop a perturbation method to describe the first few high-frequency instabilities away from the origin, present in the spectrum of the linearization about the small-amplitude Stokes waves. Asymptotic and numerical computations of these instabilities are compared for the first time to excellent agreement.

Keywords: Euler's equations, Stokes waves, spectral instability, high-frequency instabilities, perturbation methods

1 Introduction

We consider periodic gravity waves along a 1D surface of an incompressible, inviscid, and irrotational fluid of arbitrary depth. These waves are governed by Euler's equations [21]-[23]

$$\phi_{xx} + \phi_{zz} = 0 \quad \text{in} \quad \{(x, z) : |x| < \pi/\kappa \text{ and } -h < z < \eta\}, \quad (1a)$$

$$\eta_t + \eta_x \phi_x = \phi_z \quad \text{on} \quad z = \eta, \quad (1b)$$

$$\phi_t + \frac{1}{2}(\phi_x^2 + \phi_z^2) + g\eta = 0 \quad \text{on} \quad z = \eta, \quad (1c)$$

$$\phi_z = 0, \quad \text{on} \quad z = -h, \quad (1d)$$

and satisfy the periodicity conditions

$$\eta(-\pi/\kappa, t) = \eta(\pi/\kappa, t), \quad (2a)$$

$$\phi_x(-\pi/\kappa, z, t) = \phi_x(\pi/\kappa, z, t), \quad \phi_z(-\pi/\kappa, z, t) = \phi_z(\pi/\kappa, z, t). \quad (2b)$$

In these equations, $\eta = \eta(x, t)$ is the surface displacement of the fluid, $\phi = \phi(x, z, t)$ is the velocity potential inside the bulk of the fluid, g is the acceleration due to gravity, h is the depth of the fluid, and κ is the wavenumber of the surface displacement, see Figure 1. Subscripts x and t denote partial differentiation.

Stokes [40] showed in 1847 that periodic, traveling-wave solutions of (1a)-(1d) in infinite depth can be expressed as a power series in a small-parameter ε that scales with the amplitude of the waves. Nekrasov [36] proved the convergence of this series in 1921, and the works of Levi-Civita [31] and Struik [41] extended these considerations to the case of finite depth, see Section 3 and Appendix A for more details.

The stability of Stokes waves with respect to longitudinal perturbations was first studied in the 1960s by Benjamin & Feir [6, 7] and Whitham [42]. These independent investigations concluded that Stokes waves are modulationally unstable, provided $\kappa h > 1.3627\dots$. This is now referred to as

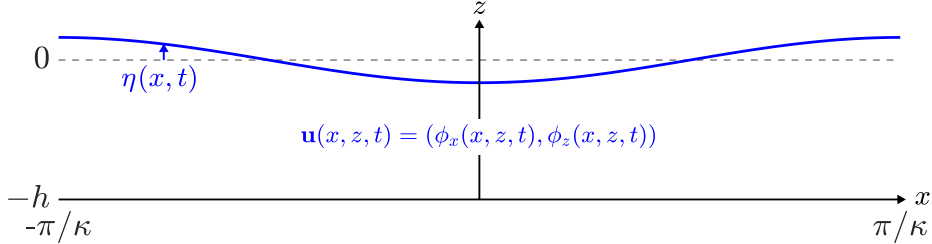


Figure 1: A schematic of 1D gravity waves in finite depth h . In this work, the surface displacement η and velocity field $\mathbf{u} = (\phi_x, \phi_z)$ are $2\pi/\kappa$ -periodic in the x -direction.

the Benjamin-Feir instability. The presence of this instability was proven rigorously in finite depth by Bridges & Mielke [9] and in infinite depth by Nguyen & Strauss [37].

In the 1970s, Bryant [10]-[11] studied the stability of Stokes waves with respect to co-periodic and transverse perturbations in shallow depth ($\kappa h < 1.3627\dots$), while Longuet-Higgins [32, 33] considered infinite depth with longitudinal perturbations that were sub- and super-harmonic to the fundamental period of the Stokes wave. McLean [35] extended this work to finite depth and transverse perturbations. Over the next decades, several papers focused on the transverse instability of Stokes waves [3, 24, 30], see also [14, 25, 43].

In 2009, using a reformulation of Euler's equations developed by Ablowitz *et al.* [1], Deconinck & Oliveras [19] numerically revisited the stability of Stokes waves with respect to quasi-periodic perturbations (parameterized by a Floquet exponent $\mu \in \mathbb{R}$), encompassing both super- and sub-harmonic perturbations. This results in a spectral problem that has a countable number of finite-multiplicity eigenvalues for each value of the Floquet exponent [29]. These eigenvalues control the exponential growth rates of the perturbations, and the union of these point spectra defines the stability spectrum of the Stokes waves, to be more precisely defined in Section 4 of this paper.

The stability spectrum depends analytically on the amplitude ε of the Stokes waves [38]. In addition, for fixed ε , the spectrum is symmetric with respect to the real and imaginary axes, since (1a)-(1d) is Hamiltonian [44]. Thus, Stokes waves are spectrally stable only when the stability spectrum is a subset of the imaginary axis. Otherwise, there exists a Floquet exponent and corresponding eigenvalue for which the perturbation grows in time.

In Figure 2, we use the Floquet-Fourier-Hill (FFH) method [17, 18] to compute stability spectra of 2π -periodic Stokes waves with amplitude $\varepsilon = 0.01$ in various depths. When $\kappa h > 1.3627\dots$, we observe the Benjamin-Feir instability as a figure-eight pattern at the origin. We also find unstable eigenvalues away from the origin, referred to as high-frequency instabilities. Unlike the Benjamin-Feir instability, high-frequency instabilities appear in the stability spectrum for all values of κh . They even dominate the Benjamin-Feir instability when $1.3627\dots < \kappa h < 1.4305\dots$ [19]. The topic of this paper is the study of these high-frequency instabilities using formal perturbation methods, as described below.

High-frequency instabilities develop from a Hamiltonian-Hopf bifurcation: a nonzero, repeated eigenvalue λ_0 of the zero-amplitude stability spectrum ($\varepsilon = 0$) [3, 20, 34] leaves the imaginary axis as the amplitude increases. When $0 < \varepsilon \ll 1$, a connected locus of unstable eigenvalues forms, which we call a high-frequency isola (red inset in Figure 2). The isola is parameterized by values of μ near μ_0 , the Floquet exponent corresponding to λ_0 .

High-frequency isolas are challenging to detect for numerical methods like FFH as they exist for narrow, specific ranges of the Floquet exponent. To complicate matters further, this narrow interval of Floquet exponents drifts from μ_0 as ε increases. In most depths, μ_0 is no longer within the interval that parameterizes the first high-frequency isola for small, positive values of ε . Therefore, to capture an isola using numerical methods, one must not only take into account the narrow interval of Floquet exponents that parameterizes the isola, but also its drift from μ_0 as ε changes (Figure 3).

In this paper, we derive formal asymptotic expressions for isolas close to the origin, both in finite and infinite depth. Specifically, for each isola we derive

- (i) an interval of Floquet exponents that is asymptotic to the interval parameterizing the isola,

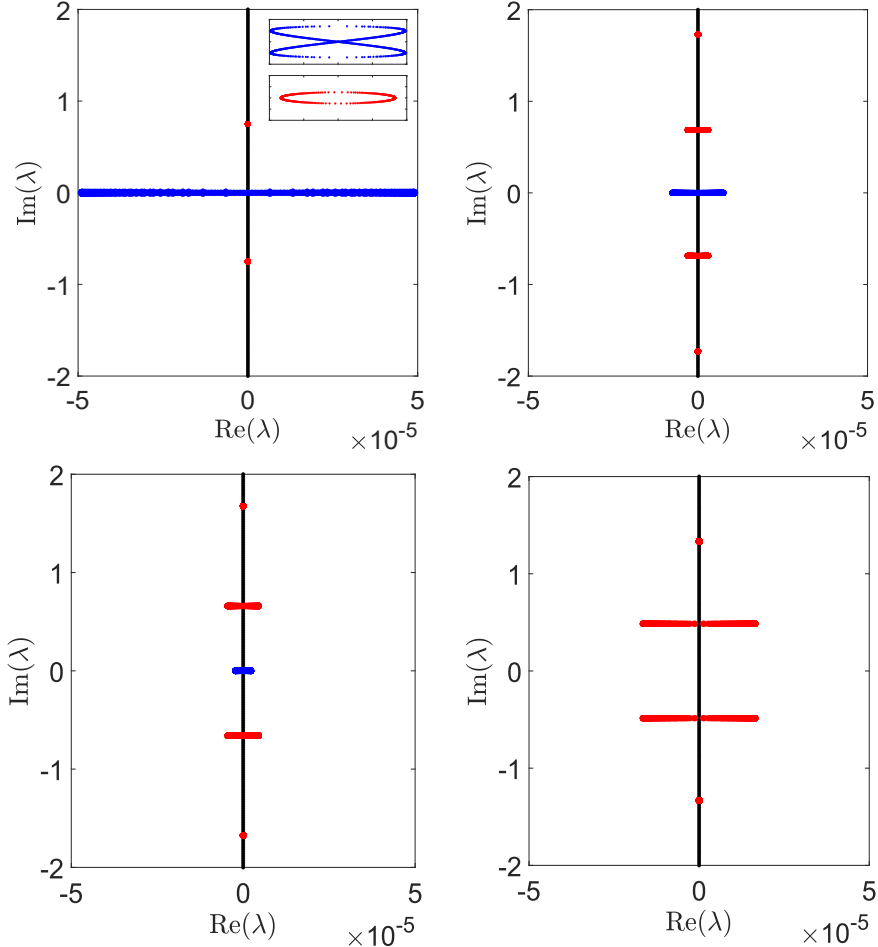


Figure 2: The stability spectrum of a 2π -periodic Stokes wave with amplitude $\varepsilon = 0.01$ and (Top, Left) $h = \infty$, (Top, Right) $h = 1.5$, (Bottom, Left) $h = 1.4$, and (Bottom, Right) $h = 1$. The Benjamin-Feir figure-eight is colored blue. The high-frequency isolas are colored red. Purely imaginary eigenvalues are colored black. A zoom-in of the Benjamin-Feir and high-frequency instabilities are inlaid in the top, left plot.

- (ii) an asymptotic expansion for the most unstable eigenvalue on the isola, and
- (iii) a closed-form expression for the curve asymptotic to the isola.

Our asymptotic expressions are compared directly with numerical results of the FFH method. For almost all κh (except a few isolated values), our asymptotic expressions predict that Stokes waves of sufficiently small (but finite) amplitude are unstable with respect to high-frequency instabilities, extending recent work by Hur & Yang [27] that establishes the instability closest to the origin only for $\kappa h \in (0.86430\dots, 1.00804\dots)$, see Section 5.

Our approach is an extension of standard eigenvalue perturbation theory [28], as we crucially let the Floquet exponent depend on the wave amplitude ε to account for the drift in the isola's Floquet parameterization. This same approach was first used in Creedon *et al.* [15] on the Kawahara equation and in Creedon *et al.* [16] on a Boussinesq-Whitham system. An outline of the leading-order calculations of the method in infinite depth is also used by Akers [5], where the emphasis is on understanding the analyticity properties of the stability spectrum as a function of the boundary conditions imposed on the perturbations (*i.e.*, as a function of the Floquet exponent), and on the connections with resonant interaction theory.

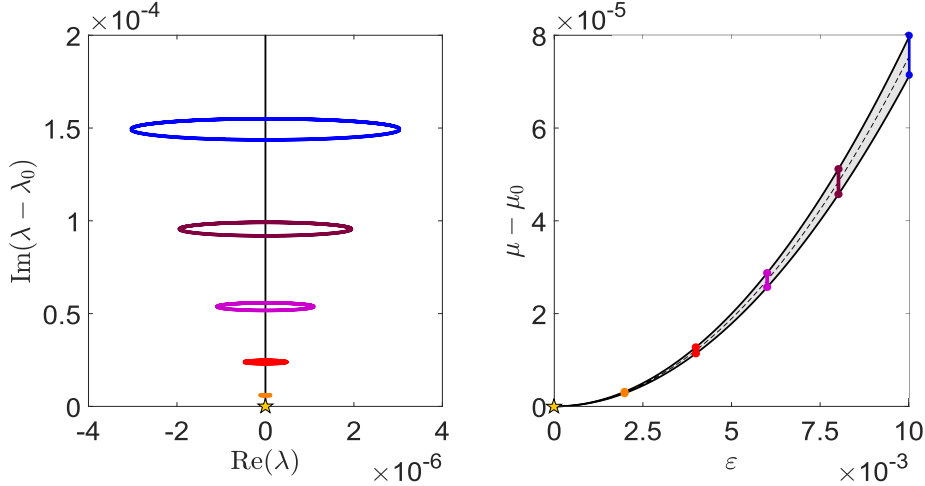


Figure 3: (Left) The high-frequency isola closest to the origin for a 2π -periodic Stokes wave in depth $h = 1.5$ with amplitude $\varepsilon = 2 \times 10^{-3}$ (orange), $\varepsilon = 4 \times 10^{-3}$ (red), $\varepsilon = 6 \times 10^{-3}$ (magenta), $\varepsilon = 8 \times 10^{-3}$ (purple), and $\varepsilon = 10^{-2}$ (blue). The imaginary axis is recentered to show the drift of the isola from the collided eigenvalues at λ_0 . The isola are computed using the perturbation method developed in this paper. (Right) The interval of Floquet exponents that parameterizes the isola closest to the origin in depth $h = 1.5$ as a function of the amplitude. The solid black lines indicate the boundaries of this interval, while the dashed black line gives the Floquet exponent corresponding to the most unstable eigenvalue on the isola. The colored lines give the Floquet exponents corresponding to the similarly colored isola in the left figure. The Floquet axis is recentered to show the drift of the parameterizing interval from the Floquet exponent μ_0 that corresponds to the collided eigenvalues. The parameterizing interval is also computed using the perturbation method in this paper.

2 The AFM Formulation

Euler's equations (1a)-(1d) together with the auxiliary conditions (2a)-(2b) constitute a boundary value problem for Laplace's equation in a domain evolving nonlinearly in time. Depending on the application, other formulations of gravity waves may be preferred over (1a)-(1d). We consider the Ablowitz-Fokas-Musslimani (AFM) formulation, first proposed in [1]. This formulation has dependence only on surface variables, as in Zakharov [44] or Craig & Sulem [13], but avoids direct numerical computations of the Dirichlet-to-Neumann operator.

As shown in [2, 39], Euler's equations (1a)-(1d) with the lateral periodic boundary conditions (2a)-(2b) are equivalent to the following system for the surface variables η and $q = \phi(x, \eta, t)$:

$$\int_{-\pi/\kappa}^{\pi/\kappa} e^{-i\kappa m x} \left[\eta_t \cosh(\kappa m (\eta + h)) + i q_x \sinh(\kappa m (\eta + h)) \right] dx = 0, \quad m \in \mathbb{Z} \setminus \{0\}, \quad (3a)$$

$$q_t + \frac{1}{2} q_x^2 + g\eta - \frac{1}{2} \frac{(\eta_t + \eta_x q_x)^2}{1 + \eta_x^2} = 0. \quad (3b)$$

We call (3a) and (3b) the nonlocal and local equations of the AFM formulation, respectively.

We write (3a)-(3b) in a traveling frame $x \rightarrow x - ct$:

$$\int_{-\pi/\kappa}^{\pi/\kappa} e^{-i\kappa m x} \left[(\eta_t - c\eta_x) \cosh(\kappa m (\eta + h)) + i q_x \sinh(\kappa m (\eta + h)) \right] dx = 0, \quad m \in \mathbb{Z} \setminus \{0\}, \quad (4a)$$

$$q_t - cq_x + \frac{1}{2} q_x^2 + g\eta - \frac{1}{2} \frac{(\eta_t - c\eta_x + \eta_x q_x)^2}{1 + \eta_x^2} = 0. \quad (4b)$$

Unless otherwise stated, x represents the horizontal coordinate in the traveling frame for the remainder of this work.

Non-dimensionalizing (4a)-(4b) according to $x \rightarrow x/\kappa$, $t \rightarrow t/\sqrt{g\kappa}$, $\eta \rightarrow \eta/\kappa$, $q \rightarrow q\sqrt{g/\kappa^3}$, $c \rightarrow c\sqrt{g/\kappa}$, and $h \rightarrow \alpha/\kappa$, we arrive at

$$\int_{-\pi}^{\pi} e^{-imx} \left[(\eta_t - c\eta_x) \cosh(m(\eta + \alpha)) + iq_x \sinh(m(\eta + \alpha)) \right] dx = 0, \quad m \in \mathbb{Z} \setminus \{0\}, \quad (5a)$$

$$q_t - cq_x + \frac{1}{2}q_x^2 + \eta - \frac{1}{2} \frac{(\eta_t - c\eta_x + \eta_x q_x)^2}{1 + \eta_x^2} = 0, \quad (5b)$$

where $\alpha = \kappa h > 0$ is the aspect ratio of the surface profile η (in dimensional variables). Without loss of generality, we study solutions of the nondimensional equations (5a)-(5b).

Remark 1. Dividing (5a) by $\cosh(m\alpha)$ and taking the limit $\alpha \rightarrow \infty$ yields (after some manipulation) the nonlocal equation in infinite depth:

$$\int_{-\pi}^{\pi} e^{-imx + |m|\eta} \left[\eta_t - c\eta_x + i \operatorname{sgn}(m) q_x \right] dx = 0, \quad m \in \mathbb{Z} \setminus \{0\}. \quad (6)$$

The local equation remains unchanged in infinite depth.

3 Small-Amplitude Stokes Waves

Using the nondimensional AFM formulation (5a)-(5b), Stokes waves are defined as surface displacements η_S and velocity potentials (at the surface) q_S that satisfy the following:

- (i) η_S and q_S are time-independent, infinitely smooth solutions of (5a)-(5b).
- (ii) η_S and $q_{S,x}$ are 2π -periodic with respect to x (but not so of q_S).
- (iii) η_S , $q_{S,x}$, and c (the velocity of the Stokes wave) depend analytically on a small parameter ε such that

$$\eta_S|_{\varepsilon=0} = 0 = q_{S,x}|_{\varepsilon=0} \quad \text{and} \quad \|\eta_S\|_{L^2} = \varepsilon + \mathcal{O}(\varepsilon^2) \quad \text{as} \quad \varepsilon \rightarrow 0.$$

- (iv) η_S and $q_{S,x}$ are even in x without loss of generality, and $c(\varepsilon)$ is even in ε .

- (v) η_S has zero average over one period.

As mentioned in the Introduction, the existence of these waves is proven in [31, 36, 41]. In this section, we derive power series expansions of η_S , $q_{S,x}$, and c in the small parameter ε using the nondimensional AFM formulation. These expansions are required for the stability calculations considered in Sections 5 and 6.

Equating time derivatives to zero in (5a)-(5b) by property (i), integrating the cosh term in (5a) by parts using property (ii), and solving for q_x in (5b), we arrive at the following equations determining the Stokes waves:

$$\int_{-\pi}^{\pi} e^{-imx} \sqrt{(1 + \eta_{S,x}^2)} (c^2 - 2\eta_S) \sinh(m(\eta_S + \alpha)) dx = 0, \quad m \in \mathbb{Z} \setminus \{0\}, \quad (7a)$$

$$q_{S,x} = c \pm \sqrt{(1 + \eta_{S,x}^2)} (c^2 - 2\eta_S). \quad (7b)$$

By property (iii), the positive branch of (7b) is defined for left-traveling waves ($c < 0$), while the negative branch is defined for right-traveling waves ($c > 0$) [12]. In what follows, we consider right-traveling waves. Similar results hold for the other case.

Remark 2. In infinite depth, (7a) becomes

$$\int_{-\pi}^{\pi} e^{-imx + |m|\eta_S} \sqrt{(1 + \eta_{S,x}^2)} (c^2 - 2\eta_S) dx = 0, \quad m \in \mathbb{Z} \setminus \{0\}. \quad (8)$$

By properties (ii) and (iv), η_S has a Fourier cosine series. We define the small-amplitude parameter ε as the first Fourier cosine mode of η_S :

$$\varepsilon = \frac{1}{\pi} \int_{-\pi}^{\pi} \eta_S \cos(x) dx. \quad (9)$$

Then, by property (iii),

$$\eta_S(x; \varepsilon) = \varepsilon \cos(x) + \mathcal{O}(\varepsilon^2), \quad (10)$$

for $|\varepsilon| \ll 1$. The leading-order term of η_S completely resolves the first Fourier cosine mode: higher-order corrections do not include terms proportional to $\cos(x)$ as a result.

Using properties (iii) and (iv), we write η_S and c as power series in ε :

$$\eta_S(x; \varepsilon) = \sum_{j=1}^{\infty} \eta_j(x) \varepsilon^j, \quad (11)$$

$$c(\varepsilon) = \sum_{j=0}^{\infty} c_{2j} \varepsilon^{2j}. \quad (12)$$

Both of these series are substituted into (7a) and, after equating powers of ε , a triangular sequence of linear integral equations for $\eta_j(x)$ and c_{2j} is found. Each of these integral equations depends on m , which can be any nonzero integer.

Remark 3. Since η_S is even in x , the integrand of (7a) modulo the complex exponential is even in x . Therefore, $m \in \mathbb{Z}^+$ without loss of generality.

The first nontrivial integral equation in this sequence is

$$\int_{-\pi}^{\pi} e^{-imx} \left[mc_0^2 \cosh(m\alpha) - \sinh(m\alpha) \right] \eta_1(x) dx = 0. \quad (13)$$

From above, $\eta_1(x) = \cos(x)$. If (13) holds for all $m \in \mathbb{Z}^+$,

$$c_0^2 = \tanh(\alpha), \quad (14)$$

otherwise (13) is not satisfied when $m = 1$. Since we study right-traveling waves, we choose $c_0 > 0$.

For the j^{th} integral equation in the sequence ($j \geq 2$), one finds

$$\eta_j(x) = \sum_{\substack{\ell=2 \\ \ell \text{ even}}}^j \hat{N}_{j,\ell} \cos(\ell x) \quad \text{for } j \text{ even}, \quad (15a)$$

$$\eta_j(x) = \sum_{\substack{\ell=3 \\ \ell \text{ odd}}}^j \hat{N}_{j,\ell} \cos(\ell x) \quad \text{for } j \text{ odd}, \quad (15b)$$

where the coefficients $\hat{N}_{j,\ell}$ are determined by the j^{th} equation with $m = \ell$. No corrections to the velocity c are found when j is even. When j is odd, c_{j-1} is determined by the j^{th} equation with $m = 1$, similar to the $j = 1$ case considered above. This correction is chosen so that $\eta_j(x)$ has no terms proportional to $\cos(x)$.

Expansions of η_S and c are substituted into (7b). After equating powers of ε , an expansion for $q_{S,x}$ follows immediately. In general,

$$q_{S,x}(x; \varepsilon) = \sum_{j=1}^{\infty} q_{j,x}(x) \varepsilon^j. \quad (16)$$

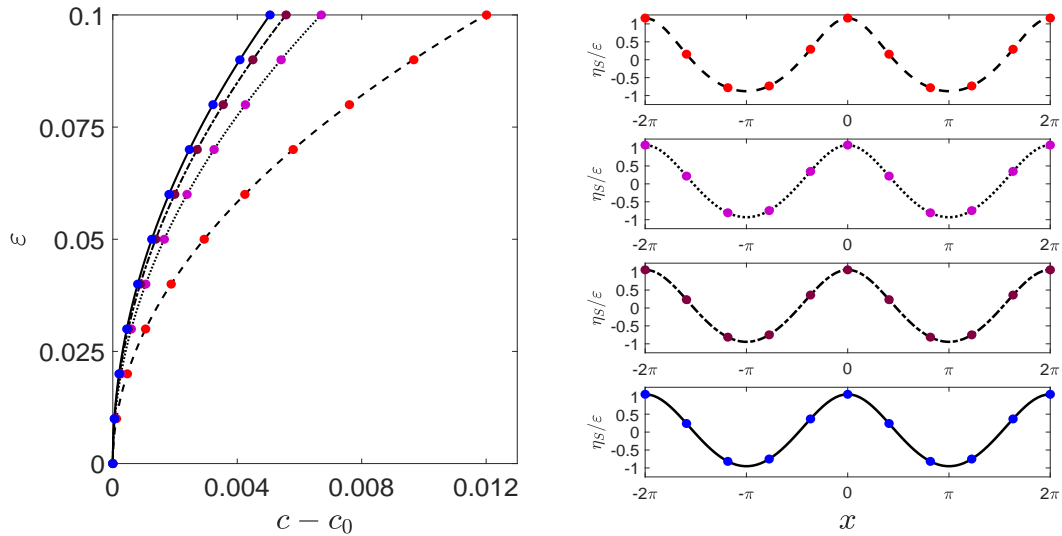


Figure 4: (Left) The amplitude *vs.* velocity bifurcation diagram of 2π -periodic Stokes waves when $\alpha = 1$ (dashed line), $\alpha = 1.5$ (dotted line), $\alpha = 2$ (dot-dashed line), and $\alpha = \infty$ (solid line), according to our $\mathcal{O}(\varepsilon^4)$ asymptotic calculations. The zeroth-order contribution c_0 is removed for better visibility. The numerical results are given by the colored dots. Red dots correspond to $\alpha = 1$, magenta dots correspond to $\alpha = 1.5$, purple dots correspond to $\alpha = 2$, and blue dots correspond to $\alpha = \infty$. (Right) Expansions of η_S/ε to $\mathcal{O}(\varepsilon^4)$ with $\varepsilon = 0.1$ for $\alpha = 1, 1.5, 2$, and ∞ (arranged from top to bottom using the same line styles as in the left figure). A sampling of the numerical results is given by the colored dots using the same color scheme as in the left figure.

The corrections $q_{j,x}(x)$ have the same structure as (15a)-(15b), but also include constant modes (when j is even) and modes proportional to $\cos(x)$ (when j is odd). Thus, $q_{S,x}$ has nonzero average, and the first Fourier cosine mode of $q_{S,x}$ has corrections beyond $\mathcal{O}(\varepsilon)$, unlike η_S .

Remark 4. Integrating (16) term-by-term gives q_S . The constant of integration can be eliminated by a Galilean transformation of (7b). Because $q_{S,x}$ has nonzero average, q_S exhibits linear growth in x . This behavior captures the mean flow induced by the traveling frame.

Explicit representations for the expansions of η_S , $q_{S,x}$, and c up to $\mathcal{O}(\varepsilon^4)$ are found in Appendix A. In Figure 4, these expansions show excellent agreement with direct numerical computations of the Stokes waves using the continuation method presented in [19].

4 The Spectral Instability of Stokes Waves

4.1 The Stability Spectrum

We consider perturbations to the Stokes waves of the form

$$\begin{pmatrix} \eta(x, t; \varepsilon, \rho) \\ q(x, t; \varepsilon, \rho) \end{pmatrix} = \begin{pmatrix} \eta_S(x; \varepsilon) \\ q_S(x; \varepsilon) \end{pmatrix} + \rho \begin{pmatrix} \eta_\rho(x, t; \varepsilon) \\ q_\rho(x, t; \varepsilon) \end{pmatrix} + \mathcal{O}(\rho^2), \quad (17)$$

where $|\rho| \ll 1$ is a parameter independent of ε . The perturbations η_ρ and q_ρ are sufficiently smooth functions of x and t that are bounded over the real line for each $t \geq 0$.

The nonlocal equation (5a) assumes η , η_t , and q_x are 2π -periodic in x , which is not required of our perturbations. We modify (5a) to allow η, η_t , and $q_x \in C^0(\mathbb{R}) \cap L^\infty(\mathbb{R})$ for each $t \geq 0$. The appropriate modification [19] is

$$\left\langle e^{-ikx} \left[(\eta_t - c\eta_x) \cosh(k(\eta + \alpha)) + iq_x \sinh(k(\eta + \alpha)) \right] \right\rangle = 0, \quad k \in \mathbb{R} \setminus \{0\}, \quad (18)$$

where

$$\langle f(x) \rangle = \lim_{L \rightarrow \infty} \frac{1}{L} \int_{-L/2}^{L/2} f(x) dx, \quad (19)$$

for any $f(x) \in C^0(\mathbb{R}) \cap L^\infty(\mathbb{R})$ [8, 19]. If η, η_t , and q_x are 2π -periodic in x for each $t \geq 0$, then (18) reduces to (5a).

Substituting (17) into (5b) and (18) and equating powers of ρ , terms of $\mathcal{O}(\rho^0)$ necessarily cancel, since η_S and q_S solve (5b) and (18). At $\mathcal{O}(\rho)$, one finds the governing equations for η_ρ and q_ρ :

$$\langle e^{-ikx} [c\mathcal{C}_k \eta_{\rho,x} + k(c\mathcal{S}_k \eta_{S,x} - i\mathcal{C}_k q_{S,x}) \eta_\rho - i\mathcal{S}_k q_{\rho,x}] \rangle = \langle e^{-ikx} \mathcal{C}_k \eta_{\rho,t} \rangle, \quad (20a)$$

$$\eta_{S,x} \zeta^2 \eta_{\rho,x} - \eta_\rho - \zeta q_{\rho,x} = q_{\rho,t} - \eta_{S,x} \zeta \eta_{\rho,t}, \quad (20b)$$

where

$$\mathcal{C}_k = \cosh(k(\eta_S + \alpha)), \quad \mathcal{S}_k = \sinh(k(\eta_S + \alpha)), \quad \zeta = \frac{q_{S,x} - c}{1 + \eta_{S,x}^2}. \quad (21)$$

Equations (20a)-(20b) are autonomous in t . We separate variables to find

$$\begin{pmatrix} \eta_\rho(x, t) \\ q_\rho(x, t) \end{pmatrix} = e^{\lambda t} \begin{pmatrix} N(x) \\ Q(x) \end{pmatrix}, \quad (22)$$

where $\lambda \in \mathbb{C}$ controls the growth rates of the perturbations. The functions $N(x)$ and $Q(x)$ satisfy

$$\langle e^{-ikx} [c\mathcal{C}_k N_x + k(c\mathcal{S}_k \eta_{S,x} - i\mathcal{C}_k q_{S,x}) N - i\mathcal{S}_k Q_x] \rangle = \lambda \langle e^{-ikx} \mathcal{C}_k N \rangle, \quad (23a)$$

$$\eta_{S,x} \zeta^2 N_x - N - \zeta Q_x = \lambda (Q - \eta_{S,x} \zeta N). \quad (23b)$$

Equations (23a)-(23b) are invariant under the shift $x \rightarrow x + 2\pi$ by the periodicity of η_S and $q_{S,x}$. Therefore, we expect the solutions N and Q to have Bloch form [19]

$$\begin{pmatrix} N(x) \\ Q(x) \end{pmatrix} = e^{i\mu x} \begin{pmatrix} \mathcal{N}(x) \\ \mathcal{Q}(x) \end{pmatrix}, \quad (24)$$

where $\mu \in \mathbb{R}$ is the Floquet exponent and \mathcal{N} and \mathcal{Q} are sufficiently smooth and 2π -periodic. Note that by redefining \mathcal{N} and \mathcal{Q} , $\mu \in [-1/2, 1/2)$, without loss of generality.

Substituting (24) into (23a)-(23b), we arrive at

$$\langle e^{-i(k-\mu)x} [c\mathcal{C}_k \mathcal{D}_x \mathcal{N} + k(c\mathcal{S}_k \eta_{S,x} - i\mathcal{C}_k q_{S,x}) \mathcal{N} - i\mathcal{S}_k \mathcal{D}_x \mathcal{Q}] \rangle = \lambda \langle e^{-i(k-\mu)x} \mathcal{C}_k \mathcal{N} \rangle, \quad (25a)$$

$$\eta_{S,x} \zeta^2 \mathcal{D}_x \mathcal{N} - \mathcal{N} - \zeta \mathcal{D}_x \mathcal{Q} = \lambda (\mathcal{Q} - \eta_{S,x} \zeta \mathcal{N}), \quad (25b)$$

where $\mathcal{D}_x = i\mu + \partial_x$.

The integrands of the averaging operators in (25a) are 2π -periodic except for the complex exponentials. These operators evaluate to zero unless $k - \mu = n \in \mathbb{Z}$ [19]. For such k , (25a) becomes

$$\langle e^{-inx} [c\mathcal{C}_{n+\mu} \mathcal{D}_x \mathcal{N} + (n + \mu)(c\mathcal{S}_{n+\mu} \eta_{S,x} - i\mathcal{C}_{n+\mu} q_{S,x}) \mathcal{N} - i\mathcal{S}_{n+\mu} \mathcal{D}_x \mathcal{Q}] \rangle = \lambda \langle e^{-inx} \mathcal{C}_{n+\mu} \mathcal{N} \rangle, \quad n \in \mathbb{Z}. \quad (26)$$

The averaging operators of (26) reduce to Fourier transforms:

$$\langle e^{-inx} f(x) \rangle = \frac{1}{2\pi} \int_{-\pi}^{\pi} e^{-inx} f(x) dx = \mathcal{F}_n[f(x)], \quad (27)$$

for any $f(x) \in L^2_{\text{per}}(-\pi, \pi)$. The inverse transform is

$$\mathcal{F}^{-1}[\{f_n\}] = \sum_{n=-\infty}^{\infty} f_n e^{inx}, \quad (28)$$

provided $\{f_n\} \in \ell^2(\mathbb{Z})$. Using the inverse transform on (26), we find

$$\begin{aligned} \sum_{n=-\infty}^{\infty} e^{inx} \mathcal{F}_n [c\mathcal{C}_{n+\mu} \mathcal{D}_x \mathcal{N} + (n+\mu)(c\mathcal{S}_{n+\mu} \eta_{S,x} - i\mathcal{C}_{n+\mu} q_{S,x}) \mathcal{N}] \\ + \sum_{n=-\infty}^{\infty} e^{inx} \mathcal{F}_n [-i\mathcal{S}_{n+\mu} \mathcal{D}_x \mathcal{Q}] = \lambda \sum_{n=-\infty}^{\infty} e^{inx} \mathcal{F}_n [\mathcal{C}_{n+\mu} \mathcal{N}]. \end{aligned} \quad (29)$$

Equations (25b) and (29) are written compactly as

$$\mathcal{L}_{\mu,\varepsilon} \mathbf{w}_{\mu,\varepsilon} = \lambda_{\mu,\varepsilon} \mathcal{R}_{\mu,\varepsilon} \mathbf{w}_{\mu,\varepsilon}, \quad (30)$$

where $\lambda = \lambda_{\mu,\varepsilon}$, $\mathbf{w}_{\mu,\varepsilon} = (\mathcal{N}, \mathcal{Q})^T$, and

$$\mathcal{L}_{\mu,\varepsilon} = \begin{pmatrix} \mathcal{L}_{\mu,\varepsilon}^{(1,1)} & \mathcal{L}_{\mu,\varepsilon}^{(1,2)} \\ \mathcal{L}_{\mu,\varepsilon}^{(2,1)} & \mathcal{L}_{\mu,\varepsilon}^{(2,2)} \end{pmatrix}, \quad \mathcal{R}_{\mu,\varepsilon} = \begin{pmatrix} \mathcal{R}_{\mu,\varepsilon}^{(1,1)} & 0 \\ \mathcal{R}_{\mu,\varepsilon}^{(2,1)} & 1 \end{pmatrix}, \quad (31)$$

$$\mathcal{L}_{\mu,\varepsilon}^{(1,1)}[\mathcal{N}] = \sum_{n=-\infty}^{\infty} e^{inx} \mathcal{F}_n [c\mathcal{C}_{n+\mu} \mathcal{D}_x \mathcal{N} + (n+\mu)(c\mathcal{S}_{n+\mu} \eta_{S,x} - i\mathcal{C}_{n+\mu} q_{S,x}) \mathcal{N}], \quad (32a)$$

$$\mathcal{L}_{\mu,\varepsilon}^{(1,2)}[\mathcal{Q}] = \sum_{n=-\infty}^{\infty} e^{inx} \mathcal{F}_n [-i\mathcal{S}_{n+\mu} \mathcal{D}_x \mathcal{Q}], \quad (32b)$$

$$\mathcal{L}_{\mu,\varepsilon}^{(2,1)}[\mathcal{N}] = \eta_{S,x} \zeta^2 \mathcal{D}_x \mathcal{N} - \mathcal{N}, \quad (32c)$$

$$\mathcal{L}_{\mu,\varepsilon}^{(2,2)}[\mathcal{Q}] = -\zeta \mathcal{D}_x \mathcal{Q}, \quad (32d)$$

$$\mathcal{R}_{\mu,\varepsilon}^{(1,1)}[\mathcal{N}] = \sum_{n=-\infty}^{\infty} e^{inx} \mathcal{F}_n [\mathcal{C}_{n+\mu} \mathcal{N}], \quad (32e)$$

$$\mathcal{R}_{\mu,\varepsilon}^{(2,1)}[\mathcal{N}] = -\eta_{S,x} \zeta \mathcal{N}. \quad (32f)$$

Equation (30) represents a two-parameter family of generalized eigenvalue problems for the linear operators $\mathcal{L}_{\mu,\varepsilon}$ and $\mathcal{R}_{\mu,\varepsilon}$.

Remark 5. In infinite depth,

$$\mathcal{L}_{\mu,\varepsilon}^{(1,1)}[\mathcal{N}] = \sum_{n=-\infty}^{\infty} e^{inx} \mathcal{F}_n [e^{|n+\mu|\eta_S} (c\mathcal{D}_x \mathcal{N} + (c\eta_{S,x}|n+\mu| - i(n+\mu)q_{S,x}) \mathcal{N})], \quad (33a)$$

$$\mathcal{L}_{\mu,\varepsilon}^{(1,2)}[\mathcal{Q}] = \sum_{n=-\infty}^{\infty} e^{inx} \mathcal{F}_n [e^{|n+\mu|\eta_S} (-i \operatorname{sgn}(n+\mu) \mathcal{D}_x \mathcal{Q})], \quad (33b)$$

$$\mathcal{R}_{\mu,\varepsilon}^{(1,1)}[\mathcal{N}] = \sum_{n=-\infty}^{\infty} e^{inx} \mathcal{F}_n [e^{|n+\mu|\eta_S} \mathcal{N}]. \quad (33c)$$

All other entries are the same as above.

The spectrum of (30) has a countable collection of finite-multiplicity eigenvalues $\lambda_{\mu,\varepsilon}$ for each μ [4, 19, 29]. The union of these eigenvalues over $\mu \in [-1/2, 1/2]$ is defined as the stability spectrum of Stokes waves with amplitude ε . If there exists $\lambda_{\mu,\varepsilon}$ for some μ such that $\Re(\lambda_{\mu,\varepsilon}) > 0$, then there exist perturbations of the Stokes waves η_ρ and q_ρ that grow exponentially in time. In this case, the Stokes waves are spectrally unstable. If no such μ and $\lambda_{\mu,\varepsilon}$ exist, the Stokes waves are spectrally stable.

4.2 Necessary Conditions for High-Frequency Instabilities

When $\varepsilon = 0$, (30) reduces to a generalized eigenvalue problem with constant coefficients:

$$\begin{pmatrix} i c_0(\mu + D) \cosh(\alpha(\mu + D)) & (\mu + D) \sinh(\alpha(\mu + D)) \\ -1 & i c_0(\mu + D) \end{pmatrix} \mathbf{w}_{\mu,0} = \lambda_{\mu,0} \begin{pmatrix} \cosh(\alpha(\mu + D)) & 0 \\ 0 & 1 \end{pmatrix} \mathbf{w}_{\mu,0}, \quad (34)$$

where $D = -i\partial_x$. The eigenvalues of (34) are

$$\lambda_{\mu,0,n}^{(\sigma)} = -i\Omega_\sigma(\mu + n), \quad \sigma = \pm 1, \quad n \in \mathbb{Z}, \quad (35)$$

with

$$\Omega_\sigma(z) = -c_0 z + \sigma\omega(z), \quad (36a)$$

$$\omega(z) = \operatorname{sgn}(z)\sqrt{z \tanh(\alpha z)}. \quad (36b)$$

Equation (36a) is the linear dispersion relation of the nondimensional Euler equations in a frame traveling with velocity c_0 . The parameter σ specifies the branch of the dispersion relation. As expected, (35) gives a countable collection of eigenvalues for each $\mu \in [-1/2, 1/2)$. These eigenvalues are purely imaginary, and therefore, the zero-amplitude Stokes waves are spectrally stable.

High-frequency instabilities develop from nonzero eigenvalues of (34) that have double (algebraic and geometric) multiplicity for a Floquet exponent μ_0 that satisfies [3, 20, 34]:

$$\lambda_{\mu_0,0,n}^{(\sigma_1)} = \lambda_{\mu_0,0,n+p}^{(\sigma_2)} \neq 0, \quad (37)$$

for $p \in \mathbb{Z} \setminus \{0\}$. Such double eigenvalues occur only if $\sigma_1 \neq \sigma_2$ and $|p| > 1$ [20]. More specifically, we have the following theorem:

Theorem 1. Let $c_0 > 0$, $\sigma_1 = 1$, and $\sigma_2 = -1$. For each $p \in \mathbb{Z} \setminus \{0, \pm 1\}$, there exists a unique Floquet exponent $\mu_{0,p} \in [-1/2, 1/2)$ and unique integer n_p such that

$$\lambda_{0,p} = \lambda_{\mu_{0,p},0,n_p}^{(1)} = \lambda_{\mu_{0,p},0,n_p+p}^{(-1)} \neq 0. \quad (38)$$

The eigenvalues have the symmetry $\lambda_{0,-p} = -\lambda_{0,p}$, and the magnitudes of the eigenvalues are strictly monotonically increasing as $|p| \rightarrow \infty$. The corresponding eigenfunctions are

$$\mathbf{w}_{0,p} = \beta_0 \left(\frac{1}{\omega(n_p + \mu_{0,p})} \right) e^{in_p x} + \gamma_0 \left(\frac{1}{\omega(n_p + p + \mu_{0,p})} \right) e^{i(n_p + p)x}, \quad (39)$$

where ω is given by (36b) and $\beta_0, \gamma_0 \in \mathbb{C} \setminus \{0\}$.

An important corollary is the following:

Corollary 1. Let $c_0 > 0$. Let $\lambda_{0,p}$ be given by (38) for some $p \in \mathbb{Z} \setminus \{0, \pm 1\}$. Then,

$$\omega(n_p + \mu_{0,p})\omega(n_p + p + \mu_{0,p}) > 0, \quad (40)$$

and

$$c_{g,1}(n_p + \mu_{0,p}) \neq c_{g,-1}(n_p + p + \mu_{0,p}), \quad (41)$$

where $c_{g,\sigma}(z)$ is the group velocity of $\Omega_\sigma(z)$, *i.e.*, $c_{g,\sigma}(z) = \Omega_{\sigma,z}(z)$.

Similar results hold if $c_0 < 0$ provided $\sigma_1 = -1$ and $\sigma_2 = 1$. See [16] for the proofs of Theorem 1 and Corollary 1.

The product (40) is equivalent to the Krein condition developed by MacKay & Saffman (1986) [34] and, in more generality, Deconinck & Trichtchenko (2017) [20]. This is a second necessary condition for high-frequency instabilities. Corollary 1 guarantees this condition is satisfied for all nonzero eigenvalues of (34) with double multiplicity. Both (40) and (45) are crucial to the formal asymptotic expansions of the high-frequency instabilities derived in Sections 5 and 6.

Remark 6. In infinite depth, $\mu_{0,p}$ and $\lambda_{0,p}$ are known explicitly. For $c_0 > 0$,

$$\mu_{0,p} = -\frac{\operatorname{sgn}(p)}{8}((-1)^p + 1), \quad (42a)$$

$$\lambda_{0,p} = i\frac{\operatorname{sgn}(p)}{4}(1 - p^2). \quad (42b)$$

These eigenvalues have the conjugate symmetry $\lambda_{0,-p} = -\lambda_{0,p}$, and $\{|\lambda_{0,p}|\}$ is strictly monotonically increasing as $|p| \rightarrow \infty$, similar to the finite-depth case.

5 First Isola. High-Frequency Instabilities: $p = 2$

We develop a perturbation method to obtain the leading-order behavior of the high-frequency isola that arises from $\lambda_{0,p}$ with $p = 2$. According to Theorem 1, this isola is the closest to the origin. We assume the spectral data of (30) corresponding to the isola vary analytically with ε , including the Floquet exponent:

$$\lambda_{\mu(\varepsilon),\varepsilon} = \lambda_{0,p} + \lambda_1\varepsilon + \lambda_2\varepsilon^2 + \mathcal{O}(\varepsilon^3), \quad (43a)$$

$$\mathbf{w}_{\mu(\varepsilon),\varepsilon} = \mathbf{w}_{0,p} + \mathbf{w}_1\varepsilon + \mathbf{w}_2\varepsilon^2 + \mathcal{O}(\varepsilon^3), \quad (43b)$$

$$\mu(\varepsilon) = \mu_{0,p} + \mu_1\varepsilon + \mu_2\varepsilon^2 + \mathcal{O}(\varepsilon^3). \quad (43c)$$

If the Floquet exponent has no dependence on ε , the expansions above are justified by standard eigenvalue perturbation theory [28], and one can find at most two eigenvalues on the isola. In contrast, by expanding the Floquet exponent as a series in ε , we asymptotically approximate all the eigenvalues on the isola for sufficiently small ε . We see below that the leading-order behavior of these eigenvalues is obtained at $\mathcal{O}(\varepsilon^2)$.

Remark 7. Choosing $p = -2$ gives the isola conjugate to the $p = 2$ isola. Thus, we choose $p = 2$ without loss of generality.

We impose the following normalization on $\mathbf{w}_{\mu(\varepsilon),\varepsilon}$:

$$\mathcal{F}_{n_p}[\mathbf{w}_{\mu(\varepsilon),\varepsilon} \cdot \mathbf{e}_1] = 1, \quad (44)$$

where $n_p \in \mathbb{Z}$ is given by Theorem 1 and $\mathbf{e}_1 = (1, 0)^T$. Then, $\beta_0 = 1$ in (39), and all subsequent corrections of $\mathbf{w}_{\mu(\varepsilon),\varepsilon}$ do not include the Fourier mode $\exp(in_p x)$ in the first component. The eigenvalue and Floquet expansions, (43a) and (43c) above, are unaffected by this normalization. For ease of notation, let $\lambda_{0,p} \rightarrow \lambda_0$, $\mathbf{w}_{0,p} \rightarrow \mathbf{w}_0$, $\mu_{0,p} \rightarrow \mu_0$, and $n_p \rightarrow n$.

Several of the asymptotic expressions that follow are suppressed for ease of readability. See the Data Availability Statement at the end of this manuscript for access to the full expressions.

5.1 The $\mathcal{O}(\varepsilon)$ Problem

Substituting expansions (43a)-(43c) into the generalized eigenvalue problem (30) and equating powers of ε , terms of $\mathcal{O}(\varepsilon^0)$ cancel by the choice of λ_0 , \mathbf{w}_0 , and μ_0 . Terms of $\mathcal{O}(\varepsilon)$ yield

$$(L_0 - \lambda_0 R_0) \mathbf{w}_1 = (\lambda_1 R_0 - (L_1 - \lambda_0 R_1)) \mathbf{w}_0, \quad (45)$$

where

$$L_j = \frac{1}{j!} \frac{\partial^j \mathcal{L}_{\mu(\varepsilon),\varepsilon}}{\partial \varepsilon^j} \Big|_{\varepsilon=0}, \quad R_j = \frac{1}{j!} \frac{\partial^j \mathcal{R}_{\mu(\varepsilon),\varepsilon}}{\partial \varepsilon^j} \Big|_{\varepsilon=0}, \quad j \in \mathbb{W}. \quad (46)$$

If (45) can be solved for \mathbf{w}_1 , the inhomogeneous terms on the RHS of (45) must be orthogonal to the nullspace of the adjoint of $L_0 - \lambda_0 R_0$ by the Fredholm alternative. A direct calculation shows

$$\text{Null} \left((L_0 - \lambda_0 R_0)^\dagger \right) = \text{Span} \left\{ \begin{pmatrix} 1 \\ -i\omega(n + \mu_0) \end{pmatrix} e^{inx}, \begin{pmatrix} 1 \\ i\omega(n + p + \mu_0) \end{pmatrix} e^{i(n+p)x} \right\}. \quad (47)$$

Hence, we impose the following solvability conditions on (45):

$$\left\langle \begin{pmatrix} 1 \\ -i\omega(n + \mu_0) \end{pmatrix} e^{inx}, (\lambda_1 R_0 - (L_1 - \lambda_0 R_1)) \mathbf{w}_0 \right\rangle = 0, \quad (48a)$$

$$\left\langle \begin{pmatrix} 1 \\ i\omega(n + p + \mu_0) \end{pmatrix} e^{i(n+p)x}, (\lambda_1 R_0 - (L_1 - \lambda_0 R_1)) \mathbf{w}_0 \right\rangle = 0, \quad (48b)$$

where $\langle \cdot, \cdot \rangle$ is the standard inner-product on $L_{\text{per}}^2(-\pi, \pi) \times L_{\text{per}}^2(-\pi, \pi)$. Simplifying both conditions, we arrive at

$$\lambda_1 + i\mu_1 c_{g,1}(n + \mu_0) = 0, \quad (49a)$$

$$\gamma_0 (\lambda_1 + i\mu_1 c_{g,-1}(n + p + \mu_0)) = 0. \quad (49b)$$

Since $\gamma_0 \neq 0$ by Theorem 1 and $c_{g,1}(n + \mu_0) \neq c_{g,-1}(n + p + \mu_0)$ by Corollary 1, we must have

$$\lambda_1 = 0 = \mu_1. \quad (50)$$

Thus no instabilities are found at $\mathcal{O}(\varepsilon)$.

Before proceeding to $\mathcal{O}(\varepsilon^2)$, we invert $L_0 - \lambda_0 R_0$ against its range to find the particular solution of \mathbf{w}_1 . Uniting the particular solution with the nullspace of $L_0 - \lambda_0 R_0$,

$$\mathbf{w}_1 = \sum_{\substack{j=n-1 \\ j \neq n, n+p}}^{n+p+1} \hat{\mathcal{W}}_{1,j} e^{ijx} + \beta_1 \left(\frac{1}{\omega(n+\mu_0)} \right) e^{inx} + \gamma_1 \left(\frac{1}{\omega(n+p+\mu_0)} \right) e^{i(n+p)x}, \quad (51)$$

where the coefficients $\hat{\mathcal{W}}_{1,j}$ depend on α (possibly through intermediate dependencies on known zeroth-order results) and at most linearly on γ_0 . The parameter $\gamma_1 \in \mathbb{C}$ is free at this order. By our choice of normalization (44), $\beta_1 = 0$. Thus,

$$\mathbf{w}_1 = \sum_{\substack{j=n-1 \\ j \neq n, n+p}}^{n+p+1} \hat{\mathcal{W}}_{1,j} e^{ijx} + \gamma_1 \left(\frac{1}{\omega(n+p+\mu_0)} \right) e^{i(n+p)x}. \quad (52)$$

5.2 The $\mathcal{O}(\varepsilon^2)$ Problem

At $\mathcal{O}(\varepsilon^2)$, the spectral problem (30) is

$$(L_0 - \lambda_0 R_0) \mathbf{w}_2 = \lambda_2 R_0 \mathbf{w}_0 - (L_1 - \lambda_0 R_1) \mathbf{w}_1 - (L_2 - \lambda_0 R_2) \mathbf{w}_0, \quad (53)$$

using (50). Proceeding as above, we obtain the solvability conditions for (53):

$$2(\lambda_2 + i\mathbf{c}_{2,1,n}) + i\gamma_0 \mathbf{s}_{2,n} = 0, \quad (54a)$$

$$2\gamma_0 (\lambda_2 + i\mathbf{c}_{2,-1,n+p}) + i\mathbf{s}_{2,n+p} = 0, \quad (54b)$$

where

$$\mathbf{c}_{2,\sigma,j} = \mu_2 c_{g,\sigma}(j + \mu_0) - \mathbf{p}_{2,j}. \quad (55)$$

The quantities $\mathbf{s}_{2,j}$ and $\mathbf{p}_{2,j}$ depend only on α (possibly through known zeroth- and first-order quantities). Using the collision condition (37), it can be shown that the product of $\mathbf{s}_{2,n}$ and $\mathbf{s}_{2,n+p}$ is related to a perfect square:

$$\mathbf{s}_{2,n} \mathbf{s}_{2,n+p} = -\frac{\mathcal{S}_2^2}{\omega(n + \mu_0) \omega(n + p + \mu_0)}, \quad (56)$$

where

$$\mathcal{S}_2 = \mathcal{T}_{2,1} + \mathcal{T}_{2,2} \hat{N}_{2,2} + \mathcal{T}_{2,3} \hat{Q}_{2,2}.$$

The expressions $\mathcal{T}_{2,j}$ are functions only of α , as are the Stokes wave corrections $\hat{N}_{2,2}$ and $\hat{Q}_{2,2}$, see Appendix A. When fully expanded, \mathcal{S}_2 consists of roughly 100 terms (depending on how it is written), but each term depends only on α . The full expression of \mathcal{S}_2 is found in the appropriate Mathematica notebook provided in the Data Availability Statement.

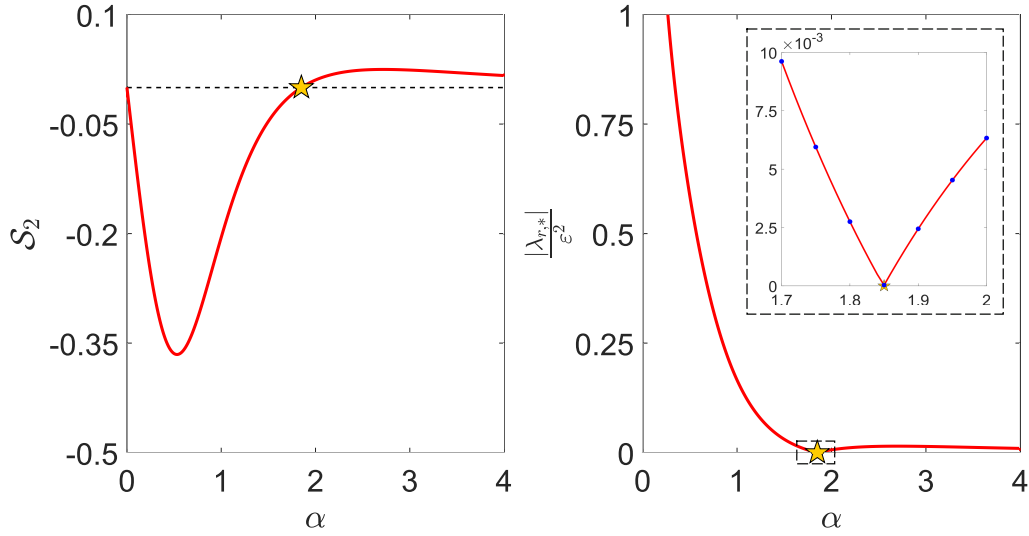


Figure 5: (Left) A plot of \mathcal{S}_2 vs. α (solid red). The zero of \mathcal{S}_2 for $\alpha > 0$ is $\alpha_1 = 1.8494040837\dots$ (gold star). (Right) The real part $\lambda_{r,*}$ of the most unstable eigenvalue on the $p = 2$ isola as a function of α according to our asymptotic calculations (solid red). The real part of the eigenvalue is normalized by ε^2 for better visibility. We zoom-in around $\alpha = \alpha_1$ (gold star) in the inlay. The real part of the most unstable eigenvalue on the isola vanishes as $\alpha \rightarrow \alpha_1$ according to our asymptotic calculations, which agrees with our numerical results using the FFH method with $\varepsilon = 0.01$ (blue dots).

Solving for λ_2 in (54a)-(54b),

$$\lambda_2 = -i \left(\frac{c_{2,-1,n+p} + c_{2,1,n}}{2} \right) \pm \sqrt{- \left(\frac{c_{2,-1,n+p} - c_{2,1,n}}{2} \right)^2 + \frac{\mathcal{S}_2^2}{4\omega(n + \mu_0)\omega(n + p + \mu_0)}}. \quad (57)$$

From Corollary 1, $\omega(n + \mu_0)\omega(n + p + \mu_0) > 0$. Thus, λ_2 has nonzero real part for $\mu_2 \in (M_{2,-}, M_{2,+})$, where

$$M_{2,\pm} = \mu_{2,*} \pm \frac{|\mathcal{S}_2|}{|c_{g,-1}(n + p + \mu_0) - c_{g,1}(n + \mu_0)| \sqrt{\omega(n + \mu_0)\omega(n + p + \mu_0)}}, \quad (58)$$

and

$$\mu_{2,*} = \frac{p_{2,n+p} - p_{2,n}}{c_{g,-1}(n + p + \mu_0) - c_{g,1}(n + \mu_0)}, \quad (59)$$

provided $\mathcal{S}_2 \neq 0$. Note that Corollary 1 guarantees (58) and (59) are well-defined, since $c_{g,-1}(n + p + \mu_0)$ and $c_{g,1}(n + \mu_0)$ are never equal.

A plot of \mathcal{S}_2 vs. α reveals that $\mathcal{S}_2 \neq 0$ except at $\alpha_1 = 1.8494040837\dots$ (Figure 5). For this isolated value of α , λ_2 has no real part at $\mathcal{O}(\varepsilon^2)$. **We conjecture that small-amplitude Stokes waves of all wavenumbers and in all depths are unstable to the high-frequency instability closest to the origin**, with the possible exception of Stokes waves with $\alpha = \alpha_1$.

To $\mathcal{O}(\varepsilon^2)$, the $p = 2$ isola is an ellipse in the complex spectral plane. The ellipse is constructed explicitly from the real and imaginary parts of

$$\lambda(\mu_2; \varepsilon) = \lambda_0 + \lambda_2(\mu_2)\varepsilon^2, \quad (60)$$

for $\mu_2 \in (M_{2,-}, M_{2,+})$. This ellipse has semi-major and -minor axes that are $\mathcal{O}(\varepsilon^2)$, and its center drifts from λ_0 along the imaginary axis like $\mathcal{O}(\varepsilon^2)$. Similarly, the interval of Floquet exponents that parameterizes this ellipse has width $\mathcal{O}(\varepsilon^2)$ and drifts from μ_0 like $\mathcal{O}(\varepsilon^2)$. In Figure 6, we compare the ellipse with a subset of numerically computed eigenvalues on the $p = 2$ isola for $\varepsilon = 0.01$ and

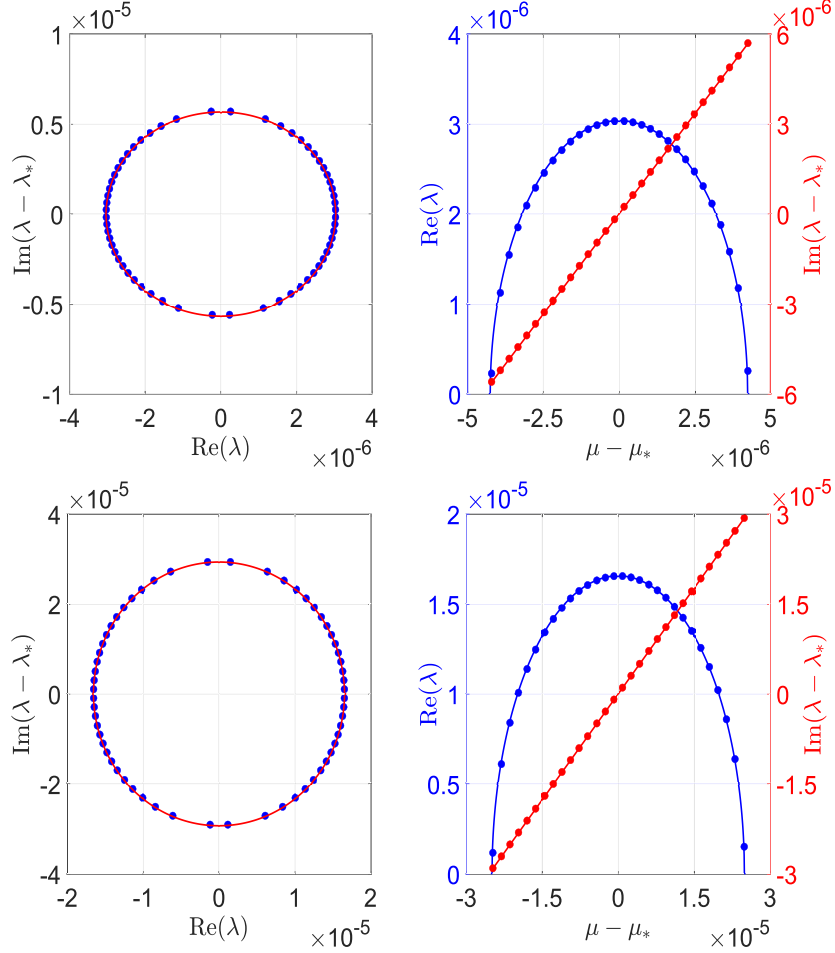


Figure 6: (Top, Left) The $p = 2$ isola with $\alpha = 1.5$ and $\varepsilon = 0.01$. The most unstable eigenvalue λ_* is removed from the imaginary axis for better visibility. The solid red curve is the ellipse obtained by our asymptotic calculations. The blue dots are a subset of eigenvalues from the numerically computed isola using the FFH method. (Top, Right) The Floquet parameterization of the real (blue) and imaginary (red) parts of the isola on the left. The most unstable eigenvalue λ_* and its corresponding Floquet exponent μ_* are removed from the imaginary and Floquet axes, respectively, for better visibility. The solid curves are our asymptotic results. The colored dots are our numerical results using the FFH method. (Bottom, Left & Right) Same with $\alpha = 1$.

find excellent agreement. We find similar agreement between the Floquet parameterization of the ellipse and of the numerically computed isola.

The eigenvalue of largest real part on the ellipse occurs when $\mu_2 = \mu_{2,*}$. Thus, the leading-order behavior of the most unstable eigenvalue on the $p = 2$ isola has real and imaginary parts

$$\lambda_{r,*} = \frac{|\mathcal{S}_2|}{2\sqrt{\omega(n + \mu_0)\omega(n + p + \mu_0)}}\varepsilon^2 + \mathcal{O}(\varepsilon^3), \quad (61a)$$

$$\lambda_{i,*} = -\Omega_1(n + \mu_0) - \left(\frac{\mathfrak{p}_{2,n+p}c_{g,1}(n + \mu_0) - \mathfrak{p}_{2,n}c_{g,-1}(n + p + \mu_0)}{c_{g,-1}(n + p + \mu_0) - c_{g,1}(n + \mu_0)} \right)\varepsilon^2 + \mathcal{O}(\varepsilon^3), \quad (61b)$$

respectively. The corresponding Floquet exponent is

$$\mu_* = \mu_0 + \mu_{2,*}\varepsilon^2 + \mathcal{O}(\varepsilon^3). \quad (62)$$

These expansions agree well with numerical results (Figure 7).

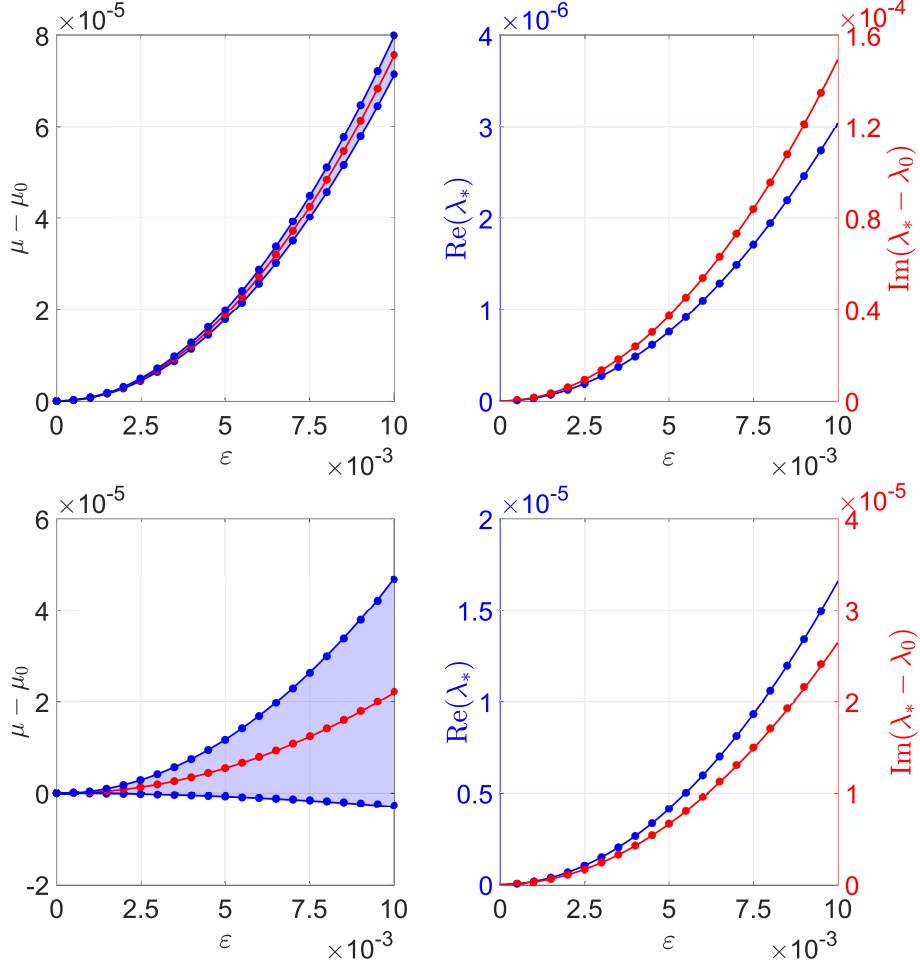


Figure 7: (Top, Left) The interval of Floquet exponents parameterizing the $p = 2$ isola as a function of ε for $\alpha = 1.5$. The zeroth-order correction of the Floquet exponent is removed from the Floquet axis for better visibility. The solid blue curves are the boundaries of this interval according to our asymptotic calculations. The blue dots are the boundaries computed numerically by the FFH method. The solid red curve gives the Floquet exponent of the most unstable eigenvalue on the isola according to our asymptotic calculations. The red dots are the Floquet exponent of the most unstable eigenvalue as computed by the FFH method. (Top, Right) The real (blue) and imaginary (red) parts of the most unstable eigenvalue of the $p = 2$ isola with $\alpha = 1.5$ as a function of ε . The zeroth-order correction of the eigenvalue is removed from the imaginary axis for better visibility. The solid curves are our asymptotic calculations. The colored dots are our numerical results using the FFH method. (Bottom, Left & Right) Same with $\alpha = 1$.

Remark 8. According to Figure 7, μ_0 is contained within the interval parameterizing the $p = 2$ isola if the boundaries of this interval have opposite concavity at $\varepsilon = 0$. This occurs if and only if $M_{2,+}M_{2,-} < 0$. In Figure 8, we plot $M_{2,+}M_{2,-}$ as a function of α . We find $M_{2,+}M_{2,-} < 0$ only if $\alpha \in (0.8643029367\dots, 1.0080416077\dots)$. Hur & Yang [27] prove the existence of an eigenvalue with Floquet exponent μ_0 on the $p = 2$ isola for α in this interval. As we have demonstrated, to account for $p = 2$ high-frequency instabilities that occur outside this interval, it is necessary to expand the Floquet exponent as a power series in ε about μ_0 .

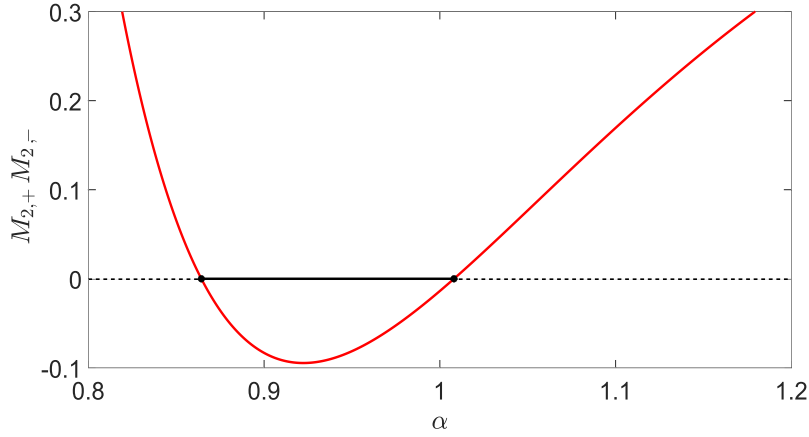


Figure 8: A plot of $M_{2,+}M_{2,-}$ vs. α (solid red). We find $M_{2,+}M_{2,-} < 0$ only when $\alpha \in (0.8643029367\dots, 1.0080416077\dots)$ (solid black). If $M_{2,+}M_{2,-} < 0$, the boundaries of the Floquet exponents parameterizing the $p = 2$ isola have opposite concavities at $\varepsilon = 0$. Only then does μ_0 remain in the interval of Floquet exponents parameterizing the isola for positive ε .

5.3 The Case of Infinite Depth

In infinite depth, the $p = 2$ isola originates from the eigenvalue

$$\lambda_0 = -\frac{3}{4}i, \quad (63)$$

with corresponding Floquet exponent $\mu_0 = -1/4$ and $n = -2$, see Remark 6. The corresponding eigenfunction, after normalizing, is

$$\mathbf{w}_0 = \begin{pmatrix} 1 \\ \frac{2}{3}i \end{pmatrix} e^{inx} + \gamma_0 \begin{pmatrix} 1 \\ -2i \end{pmatrix} e^{i(n+p)x}, \quad (64)$$

where $\gamma_0 \in \mathbb{C} \setminus \{0\}$. We modify the generalized eigenvalue problem (30) according to Remark 5 and expand the spectral data as a power series in ε about the values above.

Terms of $\mathcal{O}(\varepsilon^0)$ cancel by construction. At $\mathcal{O}(\varepsilon)$, the solvability conditions simplify to

$$\lambda_1 = 0 = \mu_1, \quad (65)$$

as in finite depth, and the normalized solution of the $\mathcal{O}(\varepsilon)$ problem is

$$\mathbf{w}_1 = \sum_{\substack{j=n-1 \\ j \neq n, n+p}}^{n+p+1} \hat{\mathcal{W}}_{1,j,\infty} e^{ijx} + \gamma_1 \begin{pmatrix} 1 \\ -2i \end{pmatrix} e^{i(n+p)x}, \quad (66)$$

where the coefficients $\hat{\mathcal{W}}_{1,j,\infty}$ depend at most linearly on γ_0 .

At $\mathcal{O}(\varepsilon^2)$, the solvability conditions are

$$\lambda_2 + i\mathbf{c}_{2,1,n,\infty} = 0, \quad (67a)$$

$$\gamma_0 (\lambda_2 + i\mathbf{c}_{2,-1,n+p,\infty}) = 0, \quad (67b)$$

where

$$\mathbf{c}_{2,\sigma,j,\infty} = \mu_2 c_{g,\sigma,\infty}(j + \mu_0) - \mathbf{p}_{2,j,\infty}, \quad (68)$$

for $c_{g,\sigma,\infty}(z) = \lim_{\alpha \rightarrow \infty} \Omega_{\sigma,z}(z)$ and explicitly computed constants $\mathbf{p}_{2,j,\infty}$.

Since $\gamma_0 \neq 0$, equations (67a)-(67b) reduce to a linear system for λ_2 and μ_2 . The solution of this system is

$$\lambda_2 = \frac{55}{32}i, \quad \mu_2 = \frac{57}{64}. \quad (69)$$

Since λ_2 is purely imaginary, the leading-order behavior of the $p = 2$ isola does not occur at $\mathcal{O}(\varepsilon^2)$, as expected from (61a), since $\lim_{\alpha \rightarrow \infty} \mathcal{S}_2 = 0$. Thus, while the asymptotic expressions involved in infinite depth are simpler than those in finite depth, **the leading-order behavior of the $p = 2$ isola requires a higher-order calculation in infinite depth.** We obtain the normalized solution of the $\mathcal{O}(\varepsilon^2)$ problem:

$$\mathbf{w}_2 = \sum_{j=n-2}^{n+p+2} \hat{\mathcal{W}}_{2,j,\infty} e^{ijx} + \gamma_2 \begin{pmatrix} 1 \\ -2i \end{pmatrix} e^{i(n+p)x}, \quad (70)$$

where the coefficients $\hat{\mathcal{W}}_{2,j,\infty}$ depend at most linearly on γ_0 and γ_1 while $\gamma_2 \in \mathbb{C}$ is a free parameter at this order.

At $\mathcal{O}(\varepsilon^3)$, the solvability conditions reduce to

$$\lambda_3 + i\mu_3 c_{g,1,\infty} (n + \mu_0) = 0, \quad (71a)$$

$$\gamma_0 (\lambda_3 + i\mu_3 c_{g,-1,\infty} (n + p + \mu_0)) = 0. \quad (71b)$$

As in finite depth, $c_{g,1,\infty} (n + \mu_0) \neq c_{g,-1,\infty} (n + p + \mu_0)$, and since $\gamma_0 \neq 0$, we must have

$$\lambda_3 = 0 = \mu_3. \quad (72)$$

No instability is observed at this order. The normalized solution of the $\mathcal{O}(\varepsilon^3)$ problem is

$$\mathbf{w}_3 = \sum_{j=n-3}^{n+p+3} \hat{\mathcal{W}}_{3,j,\infty} e^{ijx} + \gamma_3 \begin{pmatrix} 1 \\ -2i \end{pmatrix} e^{i(n+p)x}, \quad (73)$$

where the coefficients $\hat{\mathcal{W}}_{3,j,\infty}$ depend at most linearly on γ_0 , γ_1 , and γ_2 while the parameter $\gamma_3 \in \mathbb{C}$ is free at this order.

At $\mathcal{O}(\varepsilon^4)$, the solvability conditions are

$$2(\lambda_4 + i\mathbf{c}_{4,1,n,\infty}) + i\gamma_0 \mathbf{s}_{4,n,\infty} = 0, \quad (74a)$$

$$2\gamma_0 (\lambda_4 + i\mathbf{c}_{4,-1,n+p,\infty}) + i\mathbf{s}_{4,n+p,\infty} = 0, \quad (74b)$$

where

$$\mathbf{c}_{4,\sigma,j,\infty} = \mu_4 c_{g,\sigma,\infty} (j + \mu_0) - \mathbf{p}_{4,j,\infty}, \quad (75)$$

and $\mathbf{s}_{4,j,\infty}$ and $\mathbf{p}_{4,j,\infty}$ are explicitly computed constants. Substituting these constants into (74a)-(74b) and solving for λ_4 , we find the explicit formula

$$\lambda_4 = \frac{(48671 + 49152\mu_4)}{36864} i \pm \frac{\sqrt{-134933977 + 291053568\mu_4 - 150994944\mu_4^2}}{18432}. \quad (76)$$

Equation (76) has nonzero real part provided

$$\mu_4 \in \left(\frac{11843}{12288} - \frac{111\sqrt{3}}{1024}, \frac{11843}{12288} + \frac{111\sqrt{3}}{1024} \right). \quad (77)$$

Thus, the $p = 2$ isola is an ellipse to $\mathcal{O}(\varepsilon^4)$ given by the real and imaginary parts of

$$\lambda(\mu_4; \varepsilon) = -\frac{3}{4}i + \frac{55}{32}i\varepsilon^2 + \lambda_4(\mu_4)\varepsilon^4, \quad (78)$$

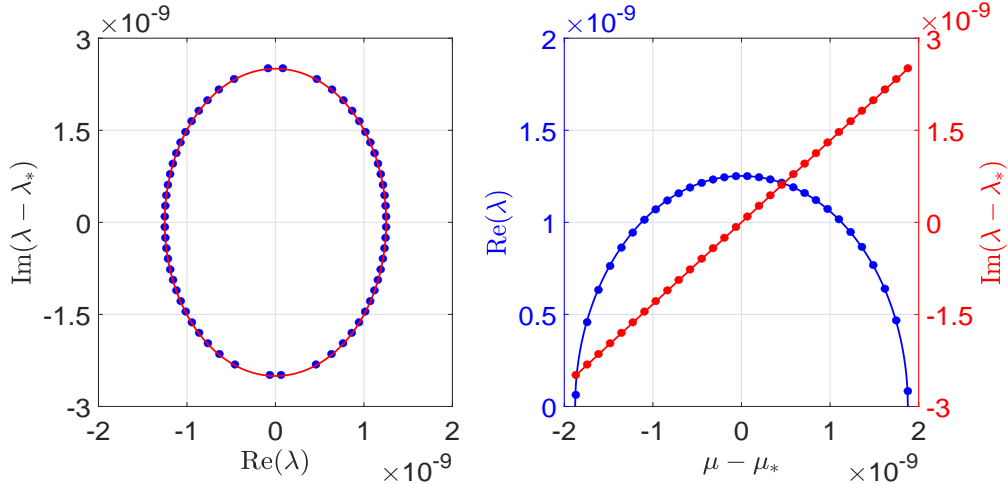


Figure 9: (Left) The $p = 2$ isola with $\alpha = \infty$ and $\varepsilon = 0.01$. The most unstable eigenvalue λ_* is removed from the imaginary axis for better visibility. The solid red curve is the ellipse obtained by our asymptotic calculations. The blue dots are a subset of eigenvalues from the numerically computed isola using the FFH method. (Right) The Floquet parameterization of the real (blue) and imaginary (red) parts of the isola. The most unstable eigenvalue λ_* and its corresponding Floquet exponent μ_* are removed from the imaginary and Floquet axes, respectively, for better visibility. The solid curves are our asymptotic results. The colored dots are our numerical results using the FFH method.

for μ_4 in (77). Unlike in finite depth, this ellipse has semi-major and -minor axes that are $\mathcal{O}(\varepsilon^4)$, while the center drifts from λ_0 like $\mathcal{O}(\varepsilon^2)$. Similarly, the Floquet parameterization of the isola has width $\mathcal{O}(\varepsilon^4)$ and drifts from μ_0 like $\mathcal{O}(\varepsilon^2)$.

In Figure 9, we compare the asymptotically computed ellipse with a subset of numerically computed eigenvalues on the $p = 2$ isola for $\varepsilon = 0.01$. Notice this ellipse is considerably smaller than that in finite depth for comparable wave amplitude (Figure 6). Excellent agreement is found between the asymptotic and numerical predictions. Similar agreement is found between the Floquet parameterization of the ellipse and of the numerically computed isola.

The eigenvalue of largest real part on the ellipse occurs when $\mu_4 = 11843/36864$. Thus, the real and imaginary parts of the most unstable eigenvalue on the isola have asymptotic expansions

$$\lambda_{r,*} = \frac{37\sqrt{3}}{512}\varepsilon^4 + \mathcal{O}(\varepsilon^5), \quad (79)$$

$$\lambda_{i,*} = -\frac{3}{4} + \frac{55}{32}\varepsilon^2 + \frac{96043}{36864}\varepsilon^4 + \mathcal{O}(\varepsilon^5), \quad (80)$$

respectively. The corresponding Floquet exponent has expansion

$$\mu_* = -\frac{1}{4} + \frac{57}{64}\varepsilon^2 + \frac{11843}{36864}\varepsilon^4 + \mathcal{O}(\varepsilon^5). \quad (81)$$

These expansions are compared with numerical results in Figure 10.

6 Second Isola. High-Frequency Instabilities: $p = 3$

We extend the perturbation method developed in Section 5 to obtain the leading-order behavior of the high-frequency isola that arises from $\lambda_{0,p}$ with $p = 3$. This isola is the second closest to the origin by Theorem 1, and its leading-order behavior is obtained at $\mathcal{O}(\varepsilon^3)$.

As in the previous section, we expand the spectral data of (30) according to (43a)-(43c) and normalize the eigenfunctions according to (44) for convenience. The perturbation method proceeds as in Section 5, with two major changes:

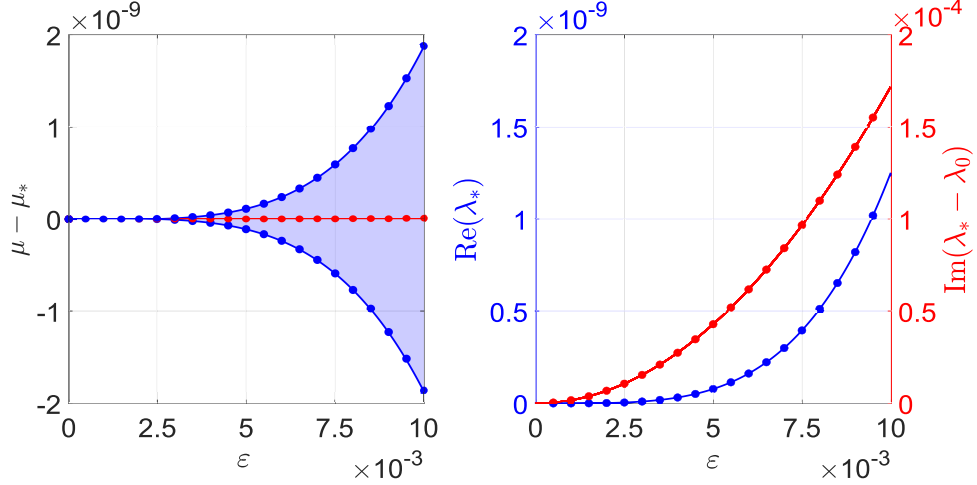


Figure 10: (Left) The interval of Floquet exponents parameterizing the $p = 2$ isola as a function of ε for $\alpha = \infty$. The most unstable Floquet exponent μ_* is removed from the Floquet axis for better visibility. The solid blue curves are the boundaries of this interval according to our asymptotic calculations. The blue dots are the boundaries computed numerically by the FFH method. The solid red curve gives the Floquet exponent of the most unstable eigenvalue on the isola according to our asymptotic calculations. The red dots are the Floquet exponent of the most unstable eigenvalue as computed by the FFH method. (Right) The real (blue) and imaginary (red) parts of the most unstable eigenvalue of the $p = 2$ isola with $\alpha = \infty$ as a function of ε . The zeroth-order correction of the eigenvalue is removed from the imaginary axis for better visibility. The solid curves are our asymptotic calculations. The colored dots are our numerical results using the FFH method.

- (i) At $\mathcal{O}(\varepsilon^2)$, the solvability conditions are independent of γ_0 and linear in λ_2 and μ_2 . As a consequence, λ_2 is purely imaginary, and the leading-order behavior of the isola is undetermined at this order.
- (ii) At $\mathcal{O}(\varepsilon^3)$, the solvability conditions depend on γ_0 , λ_3 , and γ_1 . Using solvability conditions from the previous order together with the collision condition (37), one shows that the dependence on γ_1 vanishes from these conditions.

A more complete description of these calculations is provided in Appendix B.

6.1 The $\mathcal{O}(\varepsilon^3)$ Problem

Solving for λ_3 in the solvability conditions at $\mathcal{O}(\varepsilon^3)$, we find

$$\lambda_3 = -i\mu_3 \left(\frac{c_{g,-1}(n+p+\mu_0) + c_{g,1}(n+\mu_0)}{2} \right) \pm \sqrt{-\mu_3^2 \left(\frac{c_{g,-1}(n+p+\mu_0) - c_{g,1}(n+\mu_0)}{2} \right)^2 + \frac{\mathcal{S}_3^2}{4\omega(n+\mu_0)\omega(n+p+\mu_0)}}. \quad (82)$$

Similar to \mathcal{S}_2 in the previous section, \mathcal{S}_3 is another lengthy expression depending only on α , see Appendix B for more details. A plot of \mathcal{S}_3 vs. α reveals $\mathcal{S}_3 \neq 0$, except at $\alpha_2 = 0.8206431673\dots$ (Figure 11). **We conjecture that Stokes waves of all wavenumbers and in all depths are unstable to the second closest high-frequency instability from the origin**, with possible exceptions if $\alpha = \alpha_2$. Since $\alpha_2 \neq \alpha_1$, Stokes waves of all wavenumbers and in all depths appear to be unstable with respect to high-frequency instabilities.

Remark 9. As $\alpha \rightarrow \infty$, $\mathcal{S}_3 \rightarrow 0$. Therefore, the leading-order behavior of the $p = 3$ isola in infinite depth is resolved at higher order, similar to the $p = 2$ case. For ε on the order of 0.01, this isola

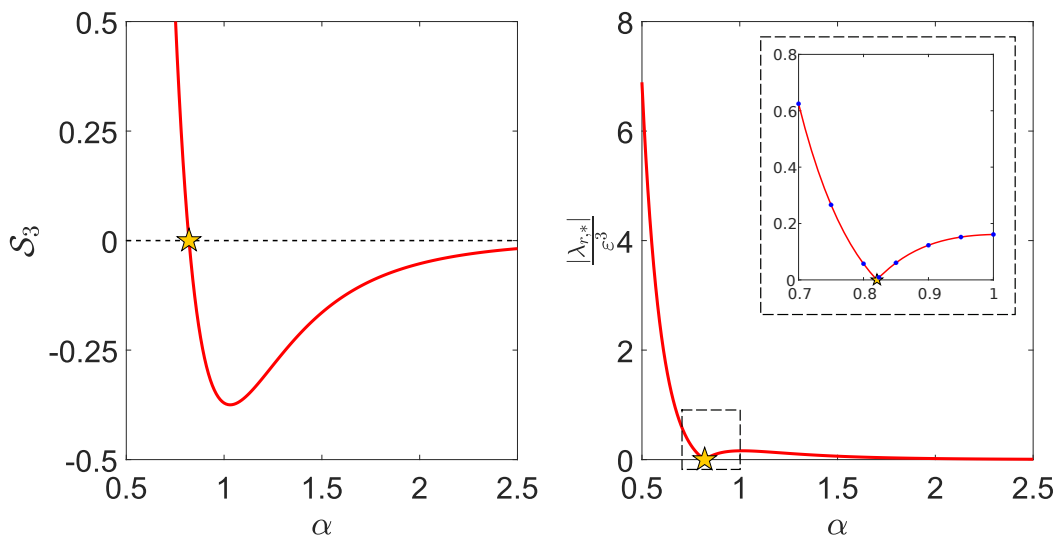


Figure 11: (Left) A plot of \mathcal{S}_3 vs. α (solid red). The zero of \mathcal{S}_3 for $\alpha > 0$ is $\alpha_2 = 0.8206431673\dots$ (gold star). (Right) The real part $\lambda_{r,*}$ of the most unstable eigenvalue on the $p = 3$ isola as a function of α according to our asymptotic calculations (solid red). The real part of the eigenvalue is normalized by ε^3 for better visibility. We zoom-in around $\alpha = \alpha_2$ (gold star) in the inlay. The real part of the most unstable eigenvalue on the isola vanishes as $\alpha \rightarrow \alpha_2$ according to our asymptotic calculations, which agrees with our numerical results using the FFH method with $\varepsilon = 0.01$ (blue dots).

is already within the numerical error of the FFH method. For larger ε , the expansions deviate too quickly from the numerics to make comparisons.

Provided $\alpha \neq \alpha_2$, (82) has nonzero real part for $\mu_3 \in (-M_3, M_3)$, where

$$M_3 = \frac{|\mathcal{S}_3|}{|c_{g,-1}(n+p+\mu_0) - c_{g,1}(n+\mu_0)|\sqrt{\omega(n+\mu_0)\omega(n+p+\mu_0)}}. \quad (83)$$

Unlike the $p = 2$ isola, this interval is symmetric about the origin. For μ_3 in this interval, the real and imaginary parts of (82), together with the lower-order corrections of λ , trace an ellipse asymptotic to the $p = 3$ isola. This ellipse has semi-major and -minor axes that scale as $\mathcal{O}(\varepsilon^3)$ and a center that drifts from λ_0 like $\mathcal{O}(\varepsilon^2)$. The Floquet parameterization of this ellipse has width $\mathcal{O}(\varepsilon^3)$ and drifts from μ_0 like $\mathcal{O}(\varepsilon^2)$. As a result, this isola is more challenging to capture than the $p = 2$ isola in finite depth.

Comparing our asymptotic and numerical $p = 3$ isolas with $\varepsilon = 0.01$ (Figure 12), we observe that, while the real part of the numerical isola matches our $\mathcal{O}(\varepsilon^3)$ calculations, the imaginary part and Floquet parameterization of the isola require fourth-order corrections. This is in contrast with the $p = 2$ isola (Figure 6), for which we obtain the drifts in the imaginary part and Floquet parameterization at the same order as the real part. We obtain these drifts for the $p = 3$ isola in the following subsection.

Equating $\mu_3 = 0$ maximizes the real part of (82). Hence, the real and imaginary part of the most unstable eigenvalue on the $p = 3$ isola have asymptotic expansions

$$\lambda_{r,*} = \left(\frac{|\mathcal{S}_3|}{2\sqrt{\omega(n+\mu_0)\omega(n+p+\mu_0)}} \right) \varepsilon^3 + \mathcal{O}(\varepsilon^4), \quad (84a)$$

$$\lambda_{i,*} = -i\Omega_1(n+\mu_0) - \left(\frac{\mathbf{p}_{2,n+p}c_{g,1}(n+\mu_0) - \mathbf{p}_{2,n}c_{g,-1}(n+p+\mu_0)}{c_{g,-1}(n+p+\mu_0) - c_{g,1}(n+\mu_0)} \right) \varepsilon^2 + \mathcal{O}(\varepsilon^4), \quad (84b)$$

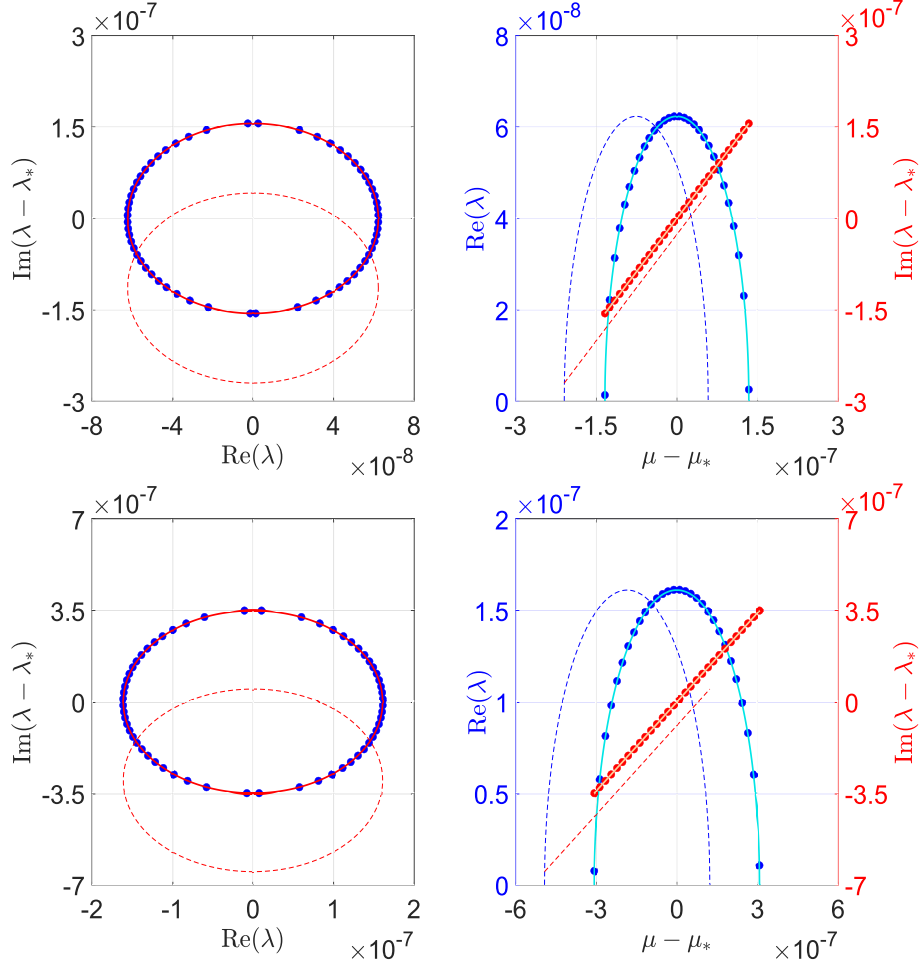


Figure 12: (Top, Left) The $p = 3$ isola with $\alpha = 1.5$ and $\varepsilon = 0.01$. The most unstable eigenvalue λ_* is removed from the imaginary axis for better visibility. The solid and dashed red curves are the ellipses obtained by our $\mathcal{O}(\varepsilon^4)$ and $\mathcal{O}(\varepsilon^3)$ asymptotic calculations, respectively. The blue dots are a subset of eigenvalues from the numerically computed isola using the FFH method. (Top, Right) The Floquet parameterization of the real (blue) and imaginary (red) parts of the isola on the left. The most unstable eigenvalue λ_* and its corresponding Floquet exponent μ_* are removed from the imaginary and Floquet axes, respectively, for better visibility. The solid teal and orange curves are our asymptotic results for the real and imaginary parts of the Floquet parameterization, respectively, to $\mathcal{O}(\varepsilon^4)$. The dashed blue and red curves are the same results to $\mathcal{O}(\varepsilon^3)$. The blue and red dots are the numerically computed real and imaginary parts of the Floquet parameterization, respectively, using the FFH method. (Bottom, Left & Right) Same with $\alpha = 1$.

respectively, and the corresponding Floquet exponent has asymptotic expansion

$$\mu_* = \mu_0 + \left(\frac{\mathfrak{p}_{2,n+p} - \mathfrak{p}_{2,n}}{c_{g,-1}(n+p+\mu_0) - c_{g,1}(n+\mu_0)} \right) \varepsilon^2 + \mathcal{O}(\varepsilon^4). \quad (85)$$

The quantities $\mathfrak{p}_{2,j}$ are defined in Appendix B.

Figure 13 compares the asymptotic expansions (84a)-(84b) and (85) with their numerical counterparts. Excellent agreement is found for the real and imaginary parts of the most unstable eigenvalue. The interval of Floquet exponents that parameterizes the isola requires a fourth-order correction to match the numerical predictions.

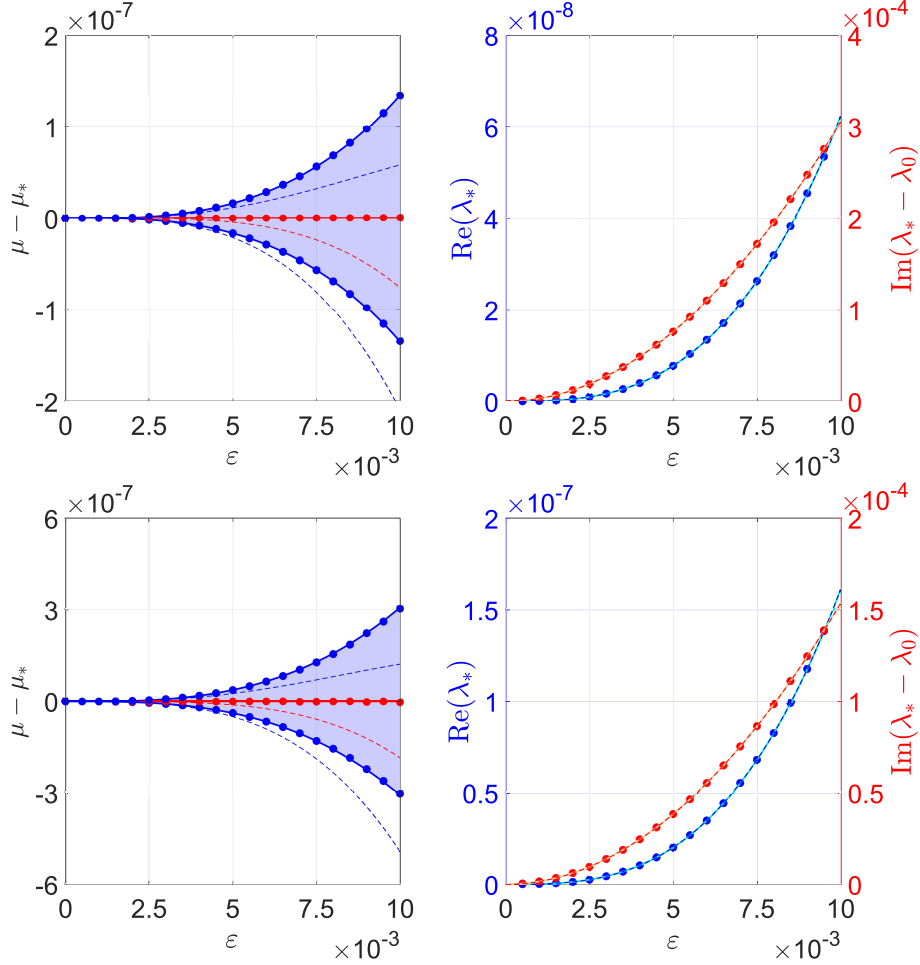


Figure 13: (Top, Left) The interval of Floquet exponents parameterizing the $p = 3$ isola as a function of ε for $\alpha = 1.5$. The most unstable Floquet exponent μ_* is removed from the Floquet axis for better visibility. The solid and dashed blue curves are the boundaries of this interval according to our $\mathcal{O}(\varepsilon^4)$ and $\mathcal{O}(\varepsilon^3)$ asymptotic calculations, respectively. The blue dots are the boundaries computed numerically by the FFH method. The solid and dashed red curves give the Floquet exponent of the most unstable eigenvalue on the isola according to our $\mathcal{O}(\varepsilon^4)$ and $\mathcal{O}(\varepsilon^3)$ asymptotic calculations, respectively. The red dots are the Floquet exponent of the most unstable eigenvalue as computed by the FFH method. (Top, Right) The real (blue) and imaginary (red) parts of the most unstable eigenvalue of the $p = 3$ isola with $\alpha = 1.5$ as a function of ε . The zeroth-order correction of the eigenvalue is removed from the imaginary axis for better visibility. The solid teal and orange curves are our asymptotic calculations for the real and imaginary parts of the most unstable eigenvalue to $\mathcal{O}(\varepsilon^4)$, respectively. The dashed blue and red curves are the same results to $\mathcal{O}(\varepsilon^3)$. The blue and red dots are the numerically computed real and imaginary parts of the most unstable eigenvalue using the FFH method. (Bottom, Left & Right) Same with $\alpha = 1$.

Before proceeding to the next order, we solve the $\mathcal{O}(\varepsilon^3)$ problem for \mathbf{w}_3 :

$$\mathbf{w}_3 = \sum_{j=n-3}^{n+p+3} \hat{\mathcal{W}}_{3,j} e^{ijx} + \gamma_3 \left(\frac{1}{\omega(n+p+\mu_0)} \right) e^{i(n+p)x}, \quad (86)$$

where the coefficients $\hat{\mathcal{W}}_{3,j}$ depend on α (possibly through intermediate dependencies on known zeroth-, first-, and second-order results) and at most linearly on γ_0, γ_1 , and γ_2 . At this order, $\gamma_3 \in \mathbb{C}$ is a free parameter.

6.2 The $\mathcal{O}(\varepsilon^4)$ Problem

At $\mathcal{O}(\varepsilon^4)$, the spectral problem (30) becomes

$$(L_0 - \lambda_0 R_0) \mathbf{w}_4 = \left(\sum_{j=0}^2 \lambda_{4-j} R_j \right) \mathbf{w}_0 + \left(\sum_{j=0}^1 \lambda_{3-j} R_j \right) \mathbf{w}_1 + \lambda_2 R_0 \mathbf{w}_2 - \sum_{j=0}^3 (L_{4-j} - \lambda_0 R_{4-j}) \mathbf{w}_j. \quad (87)$$

After some manipulation, the solvability conditions of (87) can be written as

$$\begin{pmatrix} 2 & i\mathfrak{s}_{3,n} \\ 2\gamma_0 & 2(\lambda_3 + i\mu_3 c_{g,-1}(n+p+\mu_0)) \end{pmatrix} \begin{pmatrix} \lambda_4 \\ \gamma_1 \end{pmatrix} + i\gamma_2 \begin{pmatrix} 0 \\ \mathfrak{t}_{4,n+p} \end{pmatrix} = -2i \begin{pmatrix} \mu_4 c_{g,1}(n+\mu_0) - \mathfrak{p}_{4,n} \\ \gamma_0 (\mu_4 c_{g,-1}(n+p+\mu_0) - \mathfrak{p}_{4,n+p}) \end{pmatrix}. \quad (88)$$

Using the solvability conditions at the previous order and the collision condition (37), one can show $\mathfrak{t}_{4,n+p} \equiv 0$. Then, (88) reduces to a linear system for λ_4 and γ_1 .

For $\mu_3 \in (-M_3, M_3)$ with M_3 given by (83), the determinant of (88) simplifies to

$$\det \begin{pmatrix} 2 & i\mathfrak{s}_{3,n} \\ 2\gamma_0 & 2(\lambda_3 + i\mu_3 c_{g,-1}(n+p+\mu_0)) \end{pmatrix} = 8\lambda_{3,r}, \quad (89)$$

where $\lambda_{3,r} = \text{Re}(\lambda_3)$. Provided $\alpha \neq \alpha_2$, (88) is invertible for all $\mu_3 \in (-M_3, M_3)$.

Solving (88) for λ_4 ,

$$\lambda_4 = i \left[\frac{(\lambda_3 + i\mu_3 c_{g,-1}(n+p+\mu_0)) (c_{g,1}(n+\mu_0) - \mathfrak{p}_{4,n})}{2\lambda_{3,r}} + \frac{(\lambda_3 + i\mu_3 c_{g,1}(n+\mu_0)) (c_{g,-1}(n+p+\mu_0) - \mathfrak{p}_{4,n+p})}{2\lambda_{3,r}} \right]. \quad (90)$$

Since $\mathfrak{p}_{4,j}, \mu_4 \in \mathbb{R}$, the real and imaginary parts of $\lambda_4 = \lambda_{4,r} + i\lambda_{4,i}$ are

$$\lambda_{4,r} = \frac{\mu_3 (c_{g,-1}(n+p+\mu_0) - c_{g,1}(n+\mu_0))}{4\lambda_{3,r}} \left[-\mu_4 (c_{g,-1}(n+p+\mu_0) - c_{g,1}(n+\mu_0)) + \mathfrak{p}_{2,n+p} - \mathfrak{p}_{2,n} \right], \quad (91a)$$

$$\lambda_{4,i} = -\frac{1}{2} \left[\mu_4 (c_{g,-1}(n+\mu_0) + c_{g,1}(n+\mu_0)) - (\mathfrak{p}_{4,n+p} + \mathfrak{p}_{4,n}) \right]. \quad (91b)$$

Given (91a)-(91b), we invoke the *regular curve condition*, first introduced in Creedon *et al.* (2021a) and Creedon *et al.* (2021b). According to this condition, all eigenvalue corrections must be bounded over the closure of $\mu_3 \in (-M_3, M_3)$. Notice $\lambda_{3,r} \rightarrow 0$ as $|\mu_3| \rightarrow M_3$. Thus, $\lambda_{4,r}$ is bounded only if

$$\mu_4 = \frac{\mathfrak{p}_{4,n+p} - \mathfrak{p}_{4,n}}{c_{g,-1}(n+p+\mu_0) - c_{g,1}(n+\mu_0)}. \quad (92)$$

Hence,

$$\lambda_4 = -i \left(\frac{\mathfrak{p}_{4,n+p} c_{g,1}(n+\mu_0) - \mathfrak{p}_{4,n} c_{g,-1}(n+p+\mu_0)}{c_{g,-1}(n+p+\mu_0) - c_{g,1}(n+\mu_0)} \right). \quad (93)$$

Remark 10. If $\alpha = \alpha_2$, then $\mathfrak{s}_{3,n} = 0$ and $\lambda_3 = 0 = \mu_3$. Applying the Fredholm alternative to (88), one arrives at (92) and (93), but the constants γ_0 and γ_1 remain arbitrary at this order.

Equations (92) and (93) give the fourth-order drifts in the Floquet parameterization and imaginary part of the $p = 3$ isola, respectively. The eigenvalues asymptotic to this isola form the ellipse

$$\lambda(\mu_3; \varepsilon) = \lambda_0 + \lambda_2 \varepsilon^2 + \lambda_3(\mu_3) \varepsilon^3 + \lambda_4 \varepsilon^4, \quad (94)$$

which agrees better with the numerically computed isola than at the previous order, see Figures 12 and 13.

7 Conclusion

Building on previous work by Akers [5] and Creedon *et al.* [15, 16], we have developed a formal perturbation method to compute high-frequency instabilities of small-amplitude Stokes wave solutions of Euler's equations in arbitrary depth. This method allows one to approximate an entire high-frequency isola, going beyond standard eigenvalue perturbation methods [28].

We explicitly obtain the leading-order behavior of the isolas closest to the origin in the complex spectral plane ($p = 2, 3$) for all depths, including

- (i) the Floquet exponents that parameterize the isola,
- (ii) the real and imaginary parts of the most unstable eigenvalue on the isola, and
- (iii) the curve asymptotic to the isola.

These expressions are compared directly with numerical computations of the isolas using the FFH method. Excellent agreement is found for the $p = 2$ isola. The $p = 3$ isola achieves similar agreement if higher-order corrections of the imaginary part and Floquet parameterization are computed using the regular curve condition, as defined in Section 6.

According to our asymptotic results, Stokes waves of all aspect ratios, except $\kappa h = \alpha_1$ and $\kappa h = \alpha_2$, are unstable to the $p = 2$ and $p = 3$ high-frequency instabilities, respectively. Stokes waves are also unstable to high-frequency instabilities in infinite depth ($h = \infty$), although this requires a higher-order calculation than in finite depth. Based on these findings, we conjecture that **Stokes waves of all depths and all wavenumbers are spectrally unstable to high-frequency instabilities**, extending recent work by Hur and Yang [27], where the existence of the $p = 2$ high-frequency instability is proven only if $\kappa h \in (0.86430\dots, 1.00804\dots)$. The effect of the high-frequency instabilities on the Stokes waves has been illustrated in [19].

The perturbation method developed in this work is readily extended to higher-order isolas ($p \geq 4$). It appears this method yields the first real-part correction of the isola at $\mathcal{O}(\varepsilon^p)$. In contrast, corrections to the imaginary part and Floquet parameterization of the isola appear at $\mathcal{O}(\varepsilon^2)$. Thus, we expect isolas further from the origin to have increasingly smaller widths, while their centers drift along the imaginary axis like $\mathcal{O}(\varepsilon^2)$.

If correct, this conjecture highlights one of the primary challenges for analytical and numerical investigations of high-frequency instabilities: each isola is smaller than the previous, and each isola drifts from its known zeroth-order behavior quickly relative to its size. Our hope is that the perturbation method developed in this work can be used as a starting point for future proofs of high-frequency instabilities as well as improvements to the numerical resolution of high-frequency isolas far away from the origin in the complex spectral plane.

A Stokes Wave Expansions

The Stokes waves of (5a)-(5b) have velocity

$$c(\varepsilon) = c_0 + c_2\varepsilon^2 + c_4\varepsilon^4 + \mathcal{O}(\varepsilon^6), \quad (95)$$

where

$$c_0^2 = \tanh(\alpha), \quad (96a)$$

$$c_2 = \frac{6 + 2 \cosh(2\alpha) + \cosh(4\alpha)}{16c_0 \sinh^3(\alpha) \cosh(\alpha)}, \quad (96b)$$

$$c_4 = \frac{212 + 55 \cosh(2\alpha) - 98 \cosh(4\alpha) - 23 \cosh(6\alpha) + 14 \cosh(8\alpha) + 2 \cosh(10\alpha)}{2048c_0 \sinh^9(\alpha) \cosh(\alpha)}, \quad (96c)$$

and take the form

$$\eta_S(x; \varepsilon) = \varepsilon \cos(x) + \varepsilon^2 \hat{N}_{2,2} \cos(2x) + \varepsilon^3 \hat{N}_{3,3} \cos(3x) + \varepsilon^4 \left(\hat{N}_{4,2} \cos(2x) + \hat{N}_{4,4} \cos(4x) \right) + \mathcal{O}(\varepsilon^5), \quad (97a)$$

$$q_{S,x}(x; \varepsilon) = \frac{\varepsilon}{c_0} \cos(x) + \varepsilon^2 \left(\hat{Q}_{2,0} + \hat{Q}_{2,2} \cos(2x) \right) + \varepsilon^3 \left(\hat{Q}_{3,0} \cos(x) + \hat{Q}_{3,3} \cos(3x) \right) + \varepsilon^4 \left(\hat{Q}_{4,0} + \hat{Q}_{4,2} \cos(2x) + \hat{Q}_{4,4} \cos(4x) \right) + \mathcal{O}(\varepsilon^5), \quad (97b)$$

where

$$\hat{N}_{2,2} = \frac{5 \cosh(\alpha) + \cosh(3\alpha)}{8 \sinh^3(\alpha)}, \quad (98a)$$

$$\hat{N}_{3,3} = \frac{3(14 + 15 \cosh(2\alpha) + 6 \cosh(4\alpha) + \cosh(6\alpha))}{256 \sinh^6(\alpha)}, \quad (98b)$$

$$\hat{N}_{4,2} = \frac{215 - 418 \cosh(2\alpha) - 472 \cosh(4\alpha) + 10 \cosh(6\alpha) + 17 \cosh(8\alpha)}{3072 c_0^2 \sinh^8(\alpha)}, \quad (98c)$$

$$\hat{N}_{4,4} = \frac{203 + 347 \cosh(2\alpha) + 158 \cosh(4\alpha) + 76 \cosh(6\alpha) + 23 \cosh(8\alpha) + 3 \cosh(10\alpha)}{768 c_0^2 (2 + 3 \cosh(2\alpha)) \sinh^8(\alpha)}, \quad (98d)$$

$$\hat{Q}_{2,0} = \frac{1}{4 \sinh^2(\alpha)}, \quad (98e)$$

$$\hat{Q}_{2,2} = \frac{3 + 2 \cosh(2\alpha) + \cosh(4\alpha)}{8 c_0 \sinh^3(\alpha) \cosh(\alpha)}, \quad (98f)$$

$$\hat{Q}_{3,1} = - \left(\frac{\cosh(2\alpha) (2 + \cosh(2\alpha))}{16 c_0 \sinh^4(\alpha)} \right), \quad (98g)$$

$$\hat{Q}_{3,3} = \frac{3(26 - 3 \cosh(2\alpha) + 10 \cosh(4\alpha) + 3 \cosh(6\alpha))}{256 c_0 \sinh^6(\alpha)}, \quad (98h)$$

$$\hat{Q}_{4,0} = \frac{48 + 47 \cosh(2\alpha) - 20 \cosh(4\alpha) - 3 \cosh(6\alpha)}{512 c_0 \sinh^7(\alpha) \cosh(\alpha)}, \quad (98i)$$

$$\hat{Q}_{4,2} = - \left(\frac{240 + 82 \cosh(2\alpha) + 688 \cosh(4\alpha) + 309 \cosh(6\alpha) - 16 \cosh(8\alpha) - 7 \cosh(10\alpha)}{6144 c_0 \sinh^9(\alpha) \cosh(\alpha)} \right), \quad (98j)$$

$$\hat{Q}_{4,4} = \frac{408 + 638 \cosh(2\alpha) + 230 \cosh(4\alpha) + 171 \cosh(6\alpha) + 124 \cosh(8\alpha) + 43 \cosh(10\alpha) + 6 \cosh(12\alpha)}{1536 c_0 (2 + 3 \cosh(2\alpha)) \sinh^9(\alpha) \cosh(\alpha)}. \quad (98k)$$

The Stokes expansions in infinite depth are obtained from the above with $\alpha \rightarrow \infty$.

B Detailed Calculations of the $p = 3$ Instability

For explicit representations of the asymptotic expressions derived in this appendix, see the Data Availability Statement at the end of this manuscript.

B.1 The $\mathcal{O}(\varepsilon)$ Problem

At $\mathcal{O}(\varepsilon)$, the spectral problem takes the form (45). The solvability conditions simplify to

$$\lambda_1 = 0 = \mu_1, \quad (99)$$

and the normalized solution of the $\mathcal{O}(\varepsilon)$ problem is

$$\mathbf{w}_1 = \sum_{\substack{j=n-1 \\ j \neq n, n+p}}^{n+p+1} \hat{\mathcal{W}}_{1,j} e^{ijx} + \gamma_1 \left(\frac{1}{\omega(n+p+\mu_0)} \right) e^{i(n+p)x}, \quad (100)$$

where the coefficients $\hat{\mathcal{W}}_{1,j}$ depend on α (possibly through intermediate dependencies on known zeroth-order results) and at most linearly on γ_0 . At this order, $\gamma_1 \in \mathbb{C}$ is a free parameter.

B.2 The $\mathcal{O}(\varepsilon^2)$ Problem

At $\mathcal{O}(\varepsilon^2)$, the spectral problem takes the form (53). The solvability conditions are

$$\lambda_2 + i\mathbf{c}_{2,1,n} = 0, \quad (101a)$$

$$\gamma_0 (\lambda_2 + i\mathbf{c}_{2,-1,n+p}) = 0, \quad (101b)$$

where $\mathbf{c}_{2,\sigma,j} = \mu_2 c_{g,\sigma}(j + \mu_0) - \mathbf{p}_{2,j}$, as in Section 5 (although the quantities $\mathbf{p}_{2,j}$ evaluate differently than those for the $p = 2$ isolas). Since $\gamma_0 \neq 0$, the solution of (101a)-(101b) is

$$\lambda_2 = -i \left(\frac{\mathbf{p}_{2,n+p} c_{g,1}(n + \mu_0) - \mathbf{p}_{2,n} c_{g,-1}(n + p + \mu_0)}{c_{g,-1}(n + p + \mu_0) - c_{g,1}(n + \mu_0)} \right), \quad (102a)$$

$$\mu_2 = \frac{\mathbf{p}_{2,n+p} - \mathbf{p}_{2,n}}{c_{g,-1}(n + p + \mu_0) - c_{g,1}(n + \mu_0)}. \quad (102b)$$

Since λ_2 is purely imaginary, no instabilities are found at this order. The normalized solution of the $\mathcal{O}(\varepsilon^2)$ problem is

$$\mathbf{w}_2 = \sum_{j=n-2}^{n+p+2} \hat{\mathcal{W}}_{2,j} e^{ijx} + \gamma_2 \left(\frac{1}{\omega(n+p+\mu_0)} \right) e^{i(n+p)x}, \quad (103)$$

where the coefficients $\hat{\mathcal{W}}_{2,j}$ depend on α (possibly through intermediate dependencies on known zeroth- and first-order results) and at most linearly on γ_0 and γ_1 . At this order, $\gamma_2 \in \mathbb{C}$ is a free parameter.

B.3 The $\mathcal{O}(\varepsilon^3)$ Problem

At $\mathcal{O}(\varepsilon^3)$, the spectral problem becomes

$$(L_0 - \lambda_0 R_0) \mathbf{w}_3 = (\lambda_2 R_1 + \lambda_3 R_0) \mathbf{w}_0 - \sum_{j=0}^2 (L_{3-j} - \lambda_0 R_{3-j}) \mathbf{w}_j, \quad (104)$$

with the aid of (99). The solvability conditions are

$$2(\lambda_3 + i\mu_3 c_{g,1}(n + \mu_0)) + i\gamma_0 \mathfrak{s}_{3,n} = 0, \quad (105a)$$

$$2\gamma_0 (\lambda_3 + i\mu_3 c_{g,-1}(n + p + \mu_0)) + i\mathfrak{s}_{3,n+p} + i\gamma_1 \mathfrak{t}_{3,n+p} = 0. \quad (105b)$$

Using the solvability conditions (101a)-(101b) and the collision condition (37), it can be shown

$$\mathfrak{t}_{3,n+p} \equiv 0. \quad (106)$$

As in the $p = 2$ case (Section 5), the product of $\mathfrak{s}_{3,n}$ and $\mathfrak{s}_{3,n+p}$ is related to a perfect square:

$$\mathfrak{s}_{3,n} \mathfrak{s}_{3,n+p} = - \frac{\mathcal{S}_3^2}{\omega(n + \mu_0) \omega(n + p + \mu)}, \quad (107)$$

where

$$\mathcal{S}_3 = \mathcal{T}_{3,1} + \mathcal{T}_{3,2} \hat{N}_{2,2} + \mathcal{T}_{3,3} \hat{Q}_{2,2} + \mathcal{T}_{3,4} \hat{N}_{3,3} + \mathcal{T}_{3,5} \hat{Q}_{3,3}. \quad (108)$$

The expressions $\mathcal{T}_{3,j}$ are functions only of α , as are the Stokes wave corrections $\hat{N}_{2,2}$, $\hat{Q}_{2,2}$, $\hat{N}_{3,3}$, and $\hat{Q}_{3,3}$, see Appendix A. When fully expanded, \mathcal{S}_3 involves several hundred terms, but each term depends only on α . The full expression of \mathcal{S}_3 can be found in the appropriate Mathematica notebook provided in the Data Availability Statement. The remaining calculations at this order appear in Section 6.

Data Availability Statement

The asymptotic expressions derived in this work can be found in the following Mathematica notebooks: *wwp_isola_p2.nb* ($p = 2$ isola in finite depth), *wwp_isola_p2_id.nb* ($p = 2$ isola in infinite depth), and *wwp_isola_p3.nb* ($p = 3$ isola in finite depth).

Acknowledgements

R.C. gratefully acknowledges funding from an ARCS Foundation Fellowship and from the Ruth Jung Chinn Fellowship in Applied Mathematics at the University of Washington.

References

- [1] M. J. Ablowitz, A. S. Fokas, and Z. H. Musslimani. On a new non-local formulation of water waves. *Journal of Fluid Mechanics*, 562: 313-343, 2006.
- [2] M. J. Ablowitz and T. S. Haut. Spectral formulation of the two fluid Euler equations with a free interface and long wave reduction. *Analysis and Applications*, 6(4): 323-348, 2008.
- [3] B. Akers and D. P. Nicholls. Spectral stability of deep two-dimensional gravity water waves: repeated eigenvalues. *SIAM Journal on Applied Mathematics*, 130(2): 81-107, 2012.
- [4] B. Akers and D. P. Nicholls. The spectrum of finite depth water waves. *European Journal of Mechanics-B/Fluids*, 46: 181-189, 2014.
- [5] B. Akers. Modulational instabilities of periodic traveling waves in deep water. *Physica D: Nonlinear Phenomena*, 300: 26-33, 2015.
- [6] T. B. Benjamin. Instability of periodic wave trains in nonlinear dispersive systems. *Proceedings of the Royal Society of London, Series A*, 299: 59-79, 1967.
- [7] T. B. Benjamin and J. E. Feir. The disintegration of wave trains on deep water. part i. theory. *Journal of Fluid Mechanics*, 27: 417-430, 1967.
- [8] H. Bohr. *Almost Periodic Functions*. Chelsea Publishing Company, New York, 1947.
- [9] T. H. Bridges and A. Mielke. A proof of the Benjamin-Feir instability. *Archive for Rational Mechanics and Analysis*, 133: 145-198, 1995.
- [10] P. J. Bryant. Stability of periodic waves in shallow water. *Journal of Fluid Mechanics*, 66: 81-96, 1974.
- [11] P. J. Bryant. Oblique instability of periodic waves in shallow water. *Journal of Fluid Mechanics*, 86: 783-792, 1978.
- [12] A. Constantin and W. A. Strauss. Pressure beneath a Stokes wave. *Communications on Pure and Applied Mathematics: A Journal Issued by the Courant Institute of Mathematical Sciences*, 63(4): 533-557, 2010.
- [13] W. Craig and C. Sulem. Numerical simulation of gravity waves. *Journal of Computational Physics*, 108(1): 73-83, 1993.
- [14] A. D. D. Craik. The origins of water wave theory. *Annual Review of Fluid Mechanics*, 36: 1-28, 2004.
- [15] R. P. Creedon, B. Deconinck, and O. Trichtchenko. High-frequency instabilities of the Kawahara equation: a perturbative approach, *arXiv:2101.06601*, 2021.

- [16] R. P. Creedon, B. Deconinck, and O. Trichtchenko. High-frequency instabilities of a Boussinesq-Whitham system, *Fluids*, 6(4): 136, 2021.
- [17] C. Curtis and B. Deconinck. On the convergence of Hill's method. *Mathematics of Computation*, 79(269): 169-187, 2010.
- [18] B. Deconinck and J. N. Kutz. Computing spectra of linear operators using the Floque-Fourier-Hill method. *Journal of Computational Physics*, 219(1): 296-321, 2006.
- [19] B. Deconinck and K. Oliveras. The instability of periodic surface gravity waves. *Journal of Fluid Mechanics*, 675: 141-167, 2011.
- [20] B. Deconinck and O. Trichtchenko. High frequency instabilities of small-amplitude solutions of Hamiltonian PDE's. *Discrete & Continuous Dynamical Systems-A*, 37(3): 1323-1358, 2017.
- [21] L. Euler. Principes généraux du mouvement des fluides. *Mémoires de L'académie des Sciences de Berlin*: 274-315, 1757.
- [22] L. Euler. Continuation des rcherches sur la théorie du mouvement des fluides. *Mémoires de L'académie des Sciences de Berlin*: 316-361, 1757.
- [23] L. Euler. Principia motus fluidorum. *Novi Commentarii Academiae Scientiarum Petropolitanae*: 271-311, 1761.
- [24] M. Francius and C. Kharif. Three-dimensional instabilities of periodic gravity waves in shallow water. *Journal of Fluid Mechanics*, 561: 417-437, 2006.
- [25] R. Grimshaw. *Nonlinear Waves in Fluids: Recent Advances and Modern Applications*. Springer, Wein, 2005.
- [26] M. Haragus and T. Kapitula. On the spectra of periodic waves for infinite-dimensional Hamiltonian systems, *Physica D: Nonlinear Phenomena*, 237(20): 2649-2671, 2008.
- [27] V. M. Hur and Z. Yang. Unstable Stokes waves. *arXiv:2010.10766*, 2020.
- [28] T. Kato. *Perturbation Theory for Linear Operators*. Springer-Verlag, Berlin, 1966.
- [29] T. Kapitula and K. Promislow. *Spectral and Dynamical Stability of Nonlinear Waves*. Springer, New York, 2013.
- [30] C. Kharif and A. Ramamonjariisoa. On the stability of gravity waves on deep water. *Journal of Fluid Mechanics*, 218: 163-170, 1990.
- [31] T. Levi-Civita. Determination rigoureuse des ondes permanentes d'ampleur finie. *Mathematische Annalen*, 93(1): 264-314, 1925.
- [32] M. S. Longuet-Higgins. The instabilities of gravity waves of finite amplitude in deep water i. superharmonics. *Proceedings of the Royal Society of London, Series A*, 360(1703): 471-488, 1978.
- [33] M. S. Longuet-Higgins. The instabilities of gravity waves of finite amplitude in deep water ii. subharmonics. *Proceedings of the Royal Society of London, Series A*, 360(1703): 489-505, 1978.
- [34] R. S. MacKay and P. G. Saffman. Stability of water waves. *Proceedings of the Royal Society of London, Series A*, 406(1830): 115-125, 1986.
- [35] J. W. McLean. Instabilities of finite-amplitude water waves, *Journal of Fluid Mechanics*, 114: 315-330, 1982.
- [36] A. I. Nekrasov. On waves of steady species. *Math. Ivanovo Voznesensky Polytechnic. Inst.*, 3: 52-65, 1921.

- [37] H. Q. Nguyen and W. A. Strauss. Proof of modulational instability of Stokes waves in deep water. *arXiv:2007.05018*, 2020.
- [38] D. P. Nicholls. Spectral stability of traveling water waves: analytic dependence of the spectrum. *Journal of Nonlinear Science*, 17(4): 369-397, 2007.
- [39] K. Oliveras. *Stability of Periodic Surface Gravity Water Waves*. Doctoral Dissertation, University of Washington, 2009.
- [40] G. G. Stokes. On the theory of oscillatory waves. *Transactions of the Cambridge Philosophical Society*, 8: 441-455, 1847.
- [41] D. Struik. Determination rigoureuse des ondes irrotationnelles periodiques dans un canalá profondeur finie. *Mathematische Annalen*, 95(1): 595-634, 1926.
- [42] G. B. Whitham. Non-linear dispersion of water waves. *Journal of Fluid Mechanics*, 27(2): 399-412, 1967.
- [43] H. C. Yuen and B. M. Lake. Instabilities of waves in deep water. *Annual Review of Fluid Mechanics*, 12(1): 303-334, 1980.
- [44] V. E. Zakharov. Stability of periodic waves of finite amplitude on the surface of a deep fluid. *Journal of Applied Mechanics and Technical Physics*, 9(2): 190-194, 1968.